NeuroImage 275 (2023) 120188

Contents lists available at ScienceDirect

NeuroImage

journal homepage: www.elsevier.com/locate/neuroimage

EEG responses induced by cerebellar TMS at rest and during visuomotor adaptation

Po-Yu Fong[a,b,c,*], Danny Spampinato[a,d], Kevin Michell[e], Marco Mancuso[f], Katlyn Brown[g], Jaime Ibáñez[a,h,i], Alessandro Di Santo[j,k], Anna Latorre[a], Kailash Bhatia[a], John C Rothwell[a], Lorenzo Rocchi[a,l]

[a] *Department of Clinical and Movement Neurosciences, UCL Queen Square Institute of Neurology, University College London, 3rd floor, 33 Queen Square, London WC1N 3BG, UK*
[b] *Division of Movement Disorders, Department of Neurology and Neuroscience Research Center, Chang Gung Memorial Hospital at Linkou, Taoyuan City, Taiwan, ROC*
[c] *Medical School, College of Medicine, Chang Gung University, Taoyuan, Taiwan, ROC*
[d] *Non-invasive Brain Stimulation Unit, IRCCS Santa Lucia Foundation,* Via *Ardeatina 306/354, Rome 00142, Italy*
[e] *UCL Queen Square Institute of Neurology, University College London, London, UK*
[f] *Department of Human Neurosciences, Sapienza University of Rome, Rome, Italy*
[g] *Department of Kinesiology, University of Waterloo, Waterloo, ON, Canada*
[h] *BSICoS group, I3A Institute, University of Zaragoza, IIS Aragón, Zaragoza, Spain*
[i] *Department of Bioengineering, Imperial College, London, UK*
[j] *NEuroMuscular Omnicentre (NEMO), Serena Onlus, AOS Monaldi, Naples, Italy*
[k] *Unit of Neurology, Department of Medicine, Campus Bio-Medico University of Rome, Rome, Italy*
[l] *Department of Medical Sciences and Public Health, University of Cagliari, Cagliari, Italy*

ARTICLE INFO

Keyword:
Cerebellar TMS
EEG
TMS evoked potential
Visuomotor adaptation
Auditory evoked potential

ABSTRACT

Background: Connections between the cerebellum and the cortex play a critical role in learning and executing complex behaviours. Dual-coil transcranial magnetic stimulation (TMS) can be used non-invasively to probe connectivity changes between the lateral cerebellum and motor cortex (M1) using the motor evoked potential as an outcome measure (cerebellar-brain inhibition, CBI). However, it gives no information about cerebellar connections to other parts of cortex.

Objectives: We used electroencephalography (EEG) to investigate whether it was possible to detect activity evoked in any areas of cortex by single-pulse TMS of the cerebellum (cerebellar TMS evoked potentials, cbTEPs). A second experiment tested if these responses were influenced by the performance of a cerebellar-dependent motor learning paradigm.

Methods: In the first series of experiments, TMS was applied over either the right or left cerebellar cortex, and scalp EEG was recorded simultaneously. Control conditions that mimicked auditory and somatosensory inputs associated with cerebellar TMS were included to identify responses due to non-cerebellar sensory stimulation. We conducted a follow-up experiment that evaluated whether cbTEPs are behaviourally sensitive by assessing individuals before and after learning a visuomotor reach adaptation task.

Results: A TMS pulse over the lateral cerebellum evoked EEG responses that could be distinguished from those caused by auditory and sensory artefacts. Significant positive (P80) and negative peaks (N110) over the contralateral frontal cerebral area were identified with a mirrored scalp distribution after left vs. right cerebellar stimulation. The P80 and N110 peaks were replicated in the cerebellar motor learning experiment and changed amplitude at different stages of learning. The change in amplitude of the P80 peak was associated with the degree of learning that individuals retained following adaptation. Due to overlap with sensory responses, the N110 should be interpreted with caution.

Conclusions: Cerebral potentials evoked by TMS of the lateral cerebellum provide a neurophysiological probe of cerebellar function that complements the existing CBI method. They may provide novel insight into mechanisms of visuomotor adaptation and other cognitive processes.

* Corresponding author at: Department of Clinical and Movement Neurosciences, UCL Queen Square Institute of Neurology, University College London, 3rd floor, 33 Queen Square, London WC1N 3BG, UK.
E-mail address: po-yu.fong.18@ucl.ac.uk (P.-Y. Fong).

https://doi.org/10.1016/j.neuroimage.2023.120188.
Received 10 January 2023; Received in revised form 17 May 2023; Accepted 22 May 2023
Available online 23 May 2023.

1. Introduction

The ability for humans to execute various daily actions smoothly requires constant communication of the cerebellum with diverse areas of the brain. Beyond the well-known role of the cerebellum in movement preparation, movement kinematics and learning, it is also clear that this structure is highly involved in non-motor behaviours, including cognition and emotion (Benagiano et al., 2018; Strata, 2015; Strick et al., 2009). Therefore, knowledge of the interactions between the cerebellum and cerebral cortex is necessary not only to understand how healthy individuals perform complex behaviours but also to give insights into the pathophysiology of neurological and psychiatric diseases.

Over the past decades, a variety of human neuroimaging (e.g., structural and functional magnetic resonance imaging (MRI); magneto- and electroencephalography (M/EEG)) and neurophysiological tools have been used to investigate interactions between the cerebellum and cortical areas (Allen et al., 2005; Du et al., 2018; Fernandez et al., 2021; Hallett et al., 2017; Palesi et al., 2017, 2015; Sasaki et al., 2022). However, each method has its limitations. For instance, brain imaging approaches are associated with high costs and low temporal resolution and cannot directly infer the directionality of changes in cerebellar activity or cerebellar-cortical interactions. Scalp-recorded EEG and MEG have a poor resolution of cerebellar electrical activity because it is located far from the scalp surface. On the other hand, dual-site, paired-pulse transcranial magnetic stimulation (TMS) can probe cerebellar-cortical pathways at millisecond resolution by stimulating the cerebellum with a TMS pulse and measuring the excitability of the motor cortex (M1) with a second pulse, a protocol termed cerebellar brain inhibition (CBI) (Spampinato et al., 2021; Ugawa et al., 1995). Such studies have examined changes in cerebellar-M1 connectivity during movement as well as before and after cerebellar-dependent motor learning. However, the method is limited to cerebellum-M1 connectivity: alternative approaches are needed to probe connectivity to other non-motor areas of the cortex. Indeed, the motor evoked potential (MEP), used to quantify the excitability of M1, only samples a small fraction of cortical output (the corticospinal tract) and may not represent a complete picture of motor cortex responsiveness to cerebellar stimulation. We argue that the cortical response evoked by cerebellar stimulation might be better quantified using EEG.

Combining TMS with simultaneous EEG recording (TMS-EEG) has increased in popularity as a method that combines high temporal (millisecond) resolution of cortical excitability with reasonable spatial resolution of its origin. TMS-evoked potentials (TEPs), which are the average EEG response to a phasic stimulus, provide a relatively simple measure of cortical excitability and connectivity (Mancuso et al., 2021; Tremblay et al., 2019).

Recently, a few reports have provided preliminary work integrating cerebellar TMS and EEG co-registration. These studies have shown promising results that suggest it is feasible to record TEPs and oscillatory activity following cerebellar stimulation, albeit with some differing results due to the selection of control conditions and stimulation parameters (Fernandez et al., 2021; Gassmann et al., 2022). In particular, Gassman and colleagues stimulated the cerebellum using a small figure-of-eight coil (F8 coil) and compared their results with multiple control conditions, including TMS of right occipital cortex, cerebellar TMS with downward currents and a sham condition that combined supramaximal electrical stimulation with TMS of the right shoulder. Although some of the results suggested that at least part of the EEG signals following cerebellar TMS reflect cerebellar input to the cortex, we argue that this conclusion might be strengthened by coupling cerebellar TMS-EEG with a visuomotor adaptation task known to modify the effectiveness of cerebellar-cortical connections (Koch et al., 2020; Spampinato and Celnik, 2021; Tzvi et al., 2021). It is also essential to note that such a combination between electrophysiology and behaviour would serve as a control for the sensory evoked potentials, which can easily contaminate TEPs obtained by cerebellar TMS (Fernandez et al., 2021; Gassmann et al., 2022). Indeed, while it is plausible to hypothesize that "true" cerebellar TEPs would be modulated by visuomotor adaptation, there is no physiological basis for assuming that EEG responses to auditory and somatosensory input by TMS would undergo similar changes.

We found that the main signature of cerebellar TEPs (cbTEPs) is a positive component peaking around 80 ms in the prefrontal area contralateral to the stimulated cerebellar hemisphere. This wave was side-specific, was not elicited by sensory stimulation alone and the visuomotor adaptation increased its amplitude. Overall, this evidence suggests that it may be possible to probe cerebellar-cortical connections with TMS-EEG.

2. Materials and methods

2.1. Participants

Thirty-two right-handed (Oldfield, 1971) (26.5 ± 7.6 years old, 15 male and 17 female) individuals without any history of neurological or psychiatric diseases, and who were not taking drugs active at the central nervous system, participated in the study after providing written informed consent. All experimental procedures were approved by the University College London Ethics Committee, were in accordance with the Declaration of Helsinki and followed international safety guidelines for non-invasive brain stimulation (Rossi et al., 2009).

2.2. Experimental design

During the experimental sessions recorded at rest, participants were seated in a comfortable chair in a quiet room, with their forearms resting on a pillow placed on their lap. For the experimental sessions that involved the motor task, subjects sat on a comfortable chair of suitable height and controlled a robot arm with their right arm. During TMS-EEG recordings, participants were instructed to fixate on a white cross displayed on a computer screen to prevent excessive eye movements. To mask the TMS-induced noise and minimize possible auditory evoked potentials (AEPs), participants wore earphones (MDR-EX110LP, Deep Bass Earphones, Sony, Japan) that continuously played a masking noise composed of white noise mixed with specific time-varying frequencies of the TMS click (Biabani et al., 2019; Casula et al., 2018; Fernandez et al., 2021; Massimini et al., 2005; Rocchi et al., 2018; ter Braack et al., 2015). The volume of the masking noise was adjusted for each participant by increasing the intensity until the TMS click could not be heard or to the maximum tolerated level (always below 90 dB) (Casula et al., 2018; Massimini et al., 2005; Rocchi et al., 2018).

In this study, we characterized EEG responses by cerebellar TMS obtained with a double-cone (DC) coil, which is the only one that can reliably produce CBI in healthy individuals (Fernandez et al., 2018; Hardwick et al., 2014; Spampinato et al., 2020a). We used several control conditions to investigate rigorously the impact of potential sources of sensory activation produced by TMS (Rocchi et al., 2021). Lastly, we investigated changes in cerebellar TEPs after a visuomotor adaptation task. A total of four different experiments were performed in this study. Experiments 1, 2, and 3 involved resting state recordings of cbTEPs. These were designed to investigate the effects of cerebellar stimulation on EEG signals recorded from the whole scalp and to isolate the contribution of direct cerebellar stimulation from that of auditory stimulation (experiment 2) and somatosensory stimulation mimicked by electrical stimulation (experiment 3) generated in the context of a cerebellar TMS pulse. Experiment 4 assessed changes in cbTEPs prior to and following different stages of a visuomotor learning task known to depend on cerebellar function (Spampinato and Celnik, 2021; Spampinato et al., 2017).

In experiment 1 (25 subjects, 27.4 ± 6.5 years old, 12 female and 13 male), we assessed EEG responses over the whole scalp after TMS was administered either to the left (LCS) or right (RCS) cerebellar hemisphere, in two separate recording blocks. In each block, CBI was also

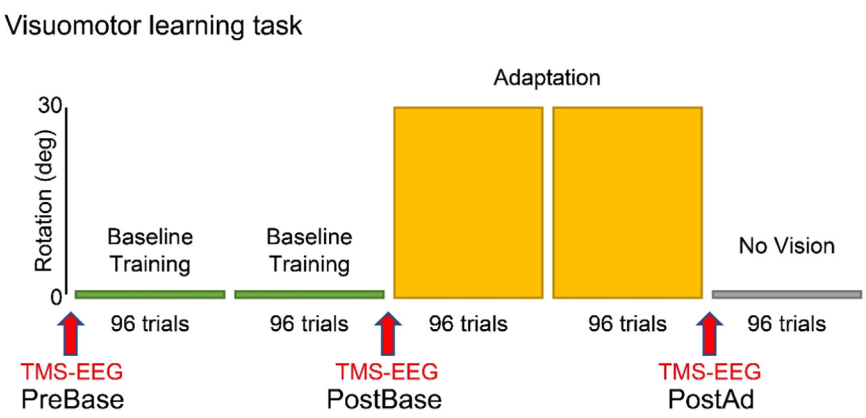

Fig. 1. Protocol of cerebellar visuomotor adaptation. The figure illustrates the sequence of reaching trial blocks and the timing of cerebellar TMS (red arrow) in experiment 4. See text for details (For interpretation of the references to color in this figure legend, the reader is referred to the web version of this article.)

measured from the first dorsal interosseous muscle (FDI) to calibrate the TMS intensity to effectively activate cerebello-cortical projections (see details in supplementary material 1). To minimize subjects' discomfort and coil overheating, each block was separated into three parts, as previously done by (Sasaki et al., 2022).

Experiments 2 and 3 were designed to control for auditory and somatosensory input, respectively, in the context of cerebellar TMS-EEG. Because previous studies offer evidence that evoked responses due to auditory and somatosensory input of TMS summate linearly (Gordon et al., 2021; Rocchi et al., 2021), we kept the two sensory stimulations delivered separately instead of combined in a realistic sham. We did this to thoroughly investigate possible EEG responses to different input modalities in cerebellar TMS, which were not previously investigated.

In experiment 2, auditory stimulation was tested (14 subjects from experiment 1, 27.7 ± 7.7 years old, 9 female and 5 male) by holding the DC coil over a 5 cm rigid spacer that provided both air-conducted and bone-conducted auditory input without directly stimulating the scalp (Conde et al., 2019; Rocchi et al., 2021). Experiment 3 was designed to mimic the broad muscle contraction induced by right cerebellar TMS (20 subjects from Experiment 1, 28.1 ± 6.7 years old, 9 female and 11 male); this was done by administering electrical stimulation simultaneously over the right masseter and trapezius muscles with two sets of electrical stimulators, as in previous work (Gordon et al., 2021).

A total of 14 subjects (25.6 ± 8.7 years old, 8 female and 6 male) were enrolled in experiment 4. First, we found a stimulation intensity to elicit reliable CBI (see details in supplementary material 1). We then delivered RCS at 3 different stages of a visuomotor learning task: prior to baseline training (PreBase), after baseline training (PostBase) and after adaptation (PostAd) (Fig. 1). In all the experiments above, each condition consisted of 100 TMS pulses, delivered at an ITI of 5 s ± 10%.

At the end of the experiments, subjects were asked to quantify loudness of the TMS click after RCS (in experiments 1 and 4) and auditory stimulation (in experiment 2), intensity of muscle twitch after RCS (in experiments 1 and 4) and somatosensory stimulation (in experiment 3), and discomfort by RCS (experiment 1 and 4) by means of a visual analog scale (VAS) with values ranging from 0 to 10 (absent to maximal perception). Of note, 14 subjects from experiment 1 were recruited in experiment 2 (auditory stimulation); since, in this condition, only auditory stimulation was delivered, only VAS scores for loudness were recorded. 20 subjects from experiment 1 participated in experiment 3 (somatosensory stimulation), where only somatosensory input was provided; Therefore, only VAS scores for twitch were recorded in experiment 3. VAS for discomfort were recorded to investigate the RCS session's tolerability; therefore, values were not used for statistical comparisons.

2.3. Cerebellar transcranial magnetic stimulation and auditory stimulation

Cerebellar stimulation was performed with a 110 mm DC coil (Rocchi et al., 2019; Spampinato et al., 2020a; Ugawa et al., 1995) (Magstim, Whitland, Dyfed, UK), located 3 cm lateral to the inion (Di Biasio et al., 2015; Monaco et al., 2018; Werhahn et al., 1996), such that current was induced upwards in the neural tissue. The choice of coil type and stimulation focus has been demonstrated to be more effective compared to F8 coils and sites above the inion (Fernandez et al., 2018; Hardwick et al., 2014; Spampinato et al., 2020a; Ugawa et al., 1995). Stimulation intensity was based on brainstem active motor threshold (AMT_{BS}) (Ugawa et al., 1995), defined as the minimum intensity able to elicit a MEP of at least 50 μV amplitude in the right preactivated the FDI muscle (i.e., during 10% of maximal voluntary contraction), with pulses given over the inion (Galea et al., 2009; Spampinato et al., 2020a). The intensity used for cerebellar stimulation was AMT_{BS} minus 5% of the maximal stimulator output (MSO) (AMT_{BS}-5%) (Schlerf et al., 2015; Ugawa et al., 1995). Twelve participants had measurable AMT_{BS} (37.5% of all participants, averaged AMT_{BS}: 66.7 ± 6.5%MSO, similar to the AMT_{BS} in previous studies (Matsumoto et al., 2008; Spampinato et al., 2020b) (see details in supplementary material 2); in those in which AMT_{BS} could not be obtained, we used the maximum tolerable intensity for cerebellar TMS – 5% MSO (maximum 80%). Table 1 lists the average stimulation intensities in each experiment.

Auditory stimulation was performed by using the same DC coil used for cerebellar stimulation, with the same cerebellar intensity in experiment 1. A 5 × 5 × 15 cm wooden rigid cuboid was placed between the DC coil and scalp to create 5 cm gap.

2.4. Somatosensory stimulation

To mimic the contraction and somatosensory input of neck and jaw muscles induced by RCS, electrical stimulation was simultaneously applied over the right masseter and trapezius muscles. For each muscle, stimulation was delivered over the middle of the muscle belly in a bipo-

Table 1
For each recording condition, intensities for TMS and somatosensory stimulation are provided. Values are expressed as MSO and mA for TMS and somatosensory stimulation, respectively. ES indicates electrical stimulation in somatosensory stimulation.

Stimulation	Average intensity	Standard deviation
Experiment 1		
RCS, LCS	66.0% MSO	7.8% MSO
Experiment 2		
RCS	68.2% MSO	6.7% MSO
Auditory stimulation	68.2% MSO	6.7% MSO
Experiment 3		
RCS	66.3% MSO	8.1% MSO
ES: right masseter muscle	15.1 mA	5.7 mA
ES: right trapezius muscle	18.8 mA	11.9 mA
Experiment 4		
RCS	63.6% MSO	7.4% MSO

lar fashion using Ag/AgCL cup electrodes. Electrodes were connected to a constant-current stimulator (DS7A, Digitimer Ltd, Welwyn Garden City, UK); monophasic square wave pulses of 200 μs duration were used. Stimulation intensities were set to produce a muscle twitch which participants subjectively judged to be matched to that generated by RCS, as in previous work (Conde et al., 2019).

2.5. Behavioural task

The behavioural task was performed on a three-degree of freedom manipulandum (3DOM) robotic interface (Klein et al., 2014). Participants sat on a chair with their forehead supported on a headrest. Their semi-pronated right hand gripped a manipulandum located underneath a horizontally suspended mirror. The mirror prevented direct vision of the hand but showed a reflection of a computer monitor mounted above that appeared to be in the same plane as the hand. Visual display of the hand was translated as an on-screen white circle cursor (0.5 cm in diameter) representing the hand, as well as a small white square target (0.7 cm x 0.7 cm) and a white home square (1.0 cm x 1.0 cm). In each trial, participants were instructed to control the cursor to make a fast-shooting movement through the presented target, thus preventing any online corrections. When the cursor passed through the invisible boundary circle (invisible circle centered on the starting position with an 8 cm radius), the cursor was hidden and participants were instructed to move back to the home square. Both the hit angle and target angle were recorded in each trial, and the angular error was calculated by the hit angle subtracting the target angle. Targets were displayed pseudo-randomly in one of eight positions located at 25, 65, 115, 155, 205, 245, 295 and 335° around the white home square.

In experiment 4, the task consisted of 5 blocks of 96 trials each. In the first two blocks (baseline training), participants were provided with online visual and end-point error feedback relative to the target position. In the following two blocks, a 30-degree anticlockwise rotation was imposed on the visual cursor that required participants to adapt their movements to hit the target accurately (adaptation). In the fifth block, the visual manipulation and visual cursor were removed to determine if individuals had learned the rotation (no vision) (Fig. 1).

2.6. Electroencephalography recording and pre-processing

EEG was recorded with a set of 63 low-profile active electrodes (ActiCap Slim, Easycap GmbH, Wörthsee, Germany) linked to a DC-coupled TMS compatible amplifier (Actichamp, Brain Products GmbH, Gilching, Germany); this technical solution has been shown to allow the recording of reliable TMS-EEG signals (Mancuso et al., 2021; Rawji et al., 2021; Rocchi et al., 2021). The scalp of each subject was prepared for EEG recording using an abrasive/conductive gel (V17 Abralyt 2000, Easycap, Herrsching, Germany). Electrode locations were based on the 10-10 international EEG system and included Fp1, Fz, F3, F7, FT9, FC5, FC1, C3, T7, TP9, CP5, CP1, Pz, P3, P7, O1, FCz, O2, P4, P8, TP10, CP6, CP2, Cz, C4, T8, FT10, FC6, FC2, F4, F8, Fp2, AF7, AF3, AFz, F1, F5, FT7, FC3, C1, C5, TP7, CP3, P1, P5, PO7, PO3, POz, PO4, PO8, P6, P2, CPz, CP4, TP8, C6, C2, FC4, FT8, F6, AF8, AF4, F2. The ground electrode was located at Fpz and the online reference was at FCz. Impedances were kept lower than 5KΩ during the whole experiment, and the sampling rate was 5000 Hz. As mentioned above, a masking noise was played during all blocks (Rocchi et al., 2021; ter Braack et al., 2015).

The EEG was pre-processed offline with analysis procedures from several open-source programs, such as EEGLab version 14.1 (Delorme and Makeig, 2004) and TMS-EEG signal analyser (TESA) toolbox (Rogasch et al., 2017), all running in MATLAB environment (Version 2015b, MathWorks, Inc., Natick, MA, United States). The raw EEG signal was first epoched from −1.3 to +1.3 s with respect to the TMS pulse, using a baseline correction from −1000 to −10 ms. The TMS artefact was removed from −5 ms to +12 ms around the TMS trigger. An independent component analysis (ICA) was then performed using a fastICA algorithm. Only the 15 components explaining the largest variance were inspected in a time window ranging from −200 to 500 ms. According to parameters such as amplitude, frequency content and scalp distribution (Rogasch et al., 2013, 2014), we removed the components which reflected EMG activity from cranial muscle and possible voltage decay. Later, the previously removed data points around the TMS artefact were interpolated with a cubic function, and the signal was downsampled (1000 Hz) and filtered with a band-pass (1–100 Hz) and band-stop (48–52 Hz) zero-phase, fourth order Butterworth filters. Epochs were restricted (from −1 to +1 s) to reduce possible edge artefacts caused by filtering, and a second round of fastICA was applied, this time focusing on residual, non-TMS-locked artefacts (e.g., continuous muscle activity, eyeblinks, lateral eye movements). At this stage, there was usually a dominant vertex N100/P200 complex, reflecting insufficient masking of auditory input (Rocchi et al., 2021). This was retained in one set of pre-processed data (i.e., RcbTEP_AEP (TEP by RCS) and LcbTEP_AEP (TEP by LCS)) and removed it in a second set (i.e., RcbTEP and LcbTEP) (see details in EEG data below). The result of auditory stimulation was named AEP and the result of somatosensory stimulation was named SEP. As a last step before the analysis, TMS-EEG signals were re-referenced to the common average reference.

2.7. Data processing and statistics

For all of the non-EEG data in this study, normality of distribution was checked by Kolmogorov-Smirnov test, and the assumption of sphericity in analysis of variance (ANOVA) was checked by Mauchly's test. Bonferroni's method was used to correct for multiple comparisons in post-hoc tests. In case of non-normal distributions, Wilcoxon signed-rank tests were used. All analyses for non-EEG data were done with SPSS version 22 (IBM, USA). P values < 0.05 were considered significant.

2.7.1. Analysis of VAS scores related to loudness of the TMS click, intensity of muscle twitch and discomfort

The average and standard deviation of VAS was calculated. A violin plot of VAS in each condition was computed and graphed by a custom script in MATLAB environment (Version 2015b, MathWorks, Inc., Natick, MA, United States) (Bastian, 2016). Two paired tests were arranged to compare the loudness score between RCS and auditory stimulation in 14 subjects and the muscle twitching between RCS and somatosensory stimulation in 20 subjects.

2.7.2. Calculation of CBI

Peak-to-peak MEP amplitudes were measured offline. Like previous studies (Fong et al., 2021; Spampinato et al., 2021; van den Hurk et al., 2007; van Elswijk et al., 2008; Wessel et al., 2019), trials containing EMG activity > 50 μV in the 100 ms preceding the TMS pulse were excluded (4.17% of all trials). CBI was calculated as the ratio of conditioned to test MEP amplitudes.

2.7.3. EEG data

2.7.3.1. Calculation of global mean field potential (GMFP) and determination of time windows of interest (ToI). After EEG pre-processing, global mean field potential (GMFP) was calculated from 13 to 250 ms after the TMS pulse and averaged across subjects, according to the formula:

$$GMFP(t) = \sqrt{\frac{\left[\sum_i^k \left(V_i(t) - V_{mean}(t)\right)^2\right]}{K}} \quad (1)$$

where, t is time (ms), K indicates the number of channels, V_i is the voltage in channel i, and V_{mean} is the averaged voltage from all channels (Casula et al., 2018; Lehmann and Skrandies, 1980; Rocchi et al., 2021). Time regions of interest (ToIs) for following statistical analyses were determined from the peaks in GMFP waveforms, separately for each comparison), as outlined in Fig. 2 and Table 2.

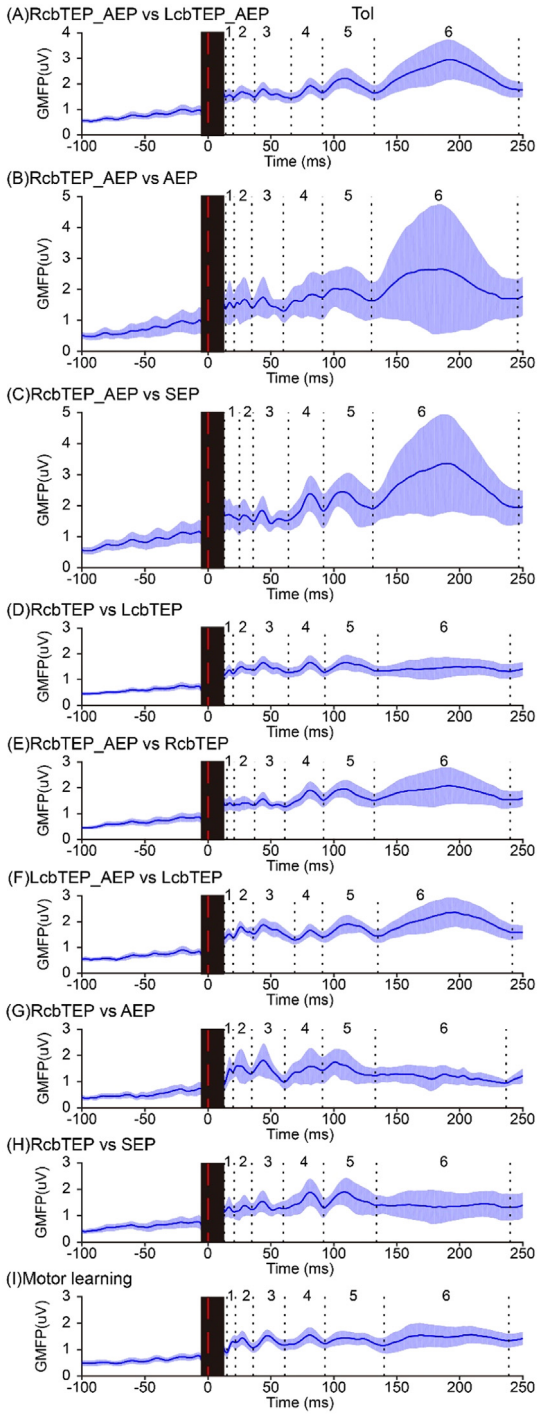

Fig. 2. GMFP. GMFPs for each analysis are plotted. ToIs boundaries are indicated with black dotted lines. The red dashed line is the time point of TMS pulse. The black panel around the TMS pulse is the time window which was cut to remove the TMS pulse artefact where the TMS pulse artefact (−5 to 12 ms). The blue areas are the 95% confidence interval of each GMFP curve. Average GMFP of RcbTEP_AEP and LcbTEP_AEP conditions (25 subjects)(A). Average GMFP of RcbTEP_AEP and AEP conditions (14 subjects)(B). Average GMFP of RcbTEP_AEP and SEP conditions (20 subjects)(C). Average GMFP of RcbTEP and LcbTEP conditions (25 subjects)(D). Average GMFP of RcbTEP_AEP and RcbTEP conditions (25 subjects)(E). Average GMFP of LcbTEP_AEP and LcbTEP conditions (25 subjects)(F). Average GMFP of RcbTEP and AEP conditions (14 subjects)(G). Average GMFP of RcbTEP and SEP conditions (20 subjects)(H). Average GMFP of the three recording blocks of experiment 4 (14 subjects)(I) (For interpretation of the references to color in this figure legend, the reader is referred to the web version of this article.)

2.7.3.2. Cerebellar TMS evoked potentials (cbTEPs) at rest. To characterize EEG responses evoked by cerebellar TMS, several paired comparisons were performed: (1) RcbTEP_AEP vs. LcbTEP_AEP, to investigate possible lateralized cortical activation after cerebellar TMS; (2) RcbTEP_AEP vs. AEP and (3) RcbTEP_AEP vs. SEP, to disentangle cbTEPs of cerebellar origin from sensory responses.

In the present experimental setting, suppression of the AEPs was difficult to obtain, because of the loud click associated with the DC coil, and the fact that the latter hindered the use of ear defenders. However, previous work has demonstrated the feasibility of offline removal of AEPs using ICA (Rogasch et al., 2014; Ross et al., 2022). Independent components reflecting AEPs were identified based on time (N100/P200 peaks) and scalp distribution (symmetrical, vertex-centered) (Rogasch et al., 2014; Ross et al., 2022); these were highly similar to signals obtained in the auditory stimulation condition (Figs. 6C and H, and S1) (Ross et al., 2022). In addition, a previous study demonstrated that auditory input is responsible for most of the N100/P200 vertex potential (Rocchi et al., 2021). It is important to note that removal of the AEP component with ICA was not expected to remove all sensory inputs, such as the SEP, that might also contribute to the N100/P200. Understanding these requires further control studies such as in experiments 2 and 3. After attenuation of N100/P200 from RcbTEP_AEP and LcbTEP_AEP (which were then named RcbTEP and LcbTEP, respectively), the second set of analyses was performed, as follows: (1) RcbTEP_AEP vs. RcbTEP and (2) LcbTEP_AEP vs. LcbTEP, to check the effect of attenuating N100/P200 and any significant impact in the signals in ToI1-ToI4; (3) RcbTEP vs. LcbTEP, similar to the analysis performed previously to explore possible lateralized cortical activation, but this time without the confounding presence of AEPs; (4) RcbTEP vs. AEP and (5) RcbTEP vs. SEP, as previously, to disentangle possible cbTEPs of cerebellar origin from sensory responses, without the confounding presence of the AEP.

2.7.3.3. cbTEPs in visuomotor learning. Analysis of cbTEPs in motor learning consisted of three pairwise comparisons: (1) PreBase vs. PostBase, to test possible changes on RcbTEPs due to motor practice, without changes in task parameters; (2) PostBase vs. PostAd, to investigate the effects of visuomotor adaptation on RcbTEPs; (3) PreBase vs. PostAad, to test net RcbTEP changes after the entire learning process.

2.7.3.4. Statistics for cbTEPs and sensory input conditions. The pairwise comparisons indicated above were performed at the scalp level by the built-in "Study" function in EEGlab (Delorme et al., 2011). Monte Carlo permutation statistics were applied and the empirical distributions for each comparison were built by permuting conditions with 1000 iterations (Maris and Oostenveld, 2007; Pernet et al., 2015). The permutations were performed in the spatio-temporal domain, including all electrodes and time points in each ToI (Opie et al., 2017; Rocchi et al., 2021; Rogasch et al., 2014). Cluster correction as implemented in Fieldtrip toolbox was used to control for type I errors (Maris and Oostenveld, 2007; Oostenveld et al., 2011). The minimal number of neighboring electrodes was two. For significant clusters (p-value < 0.05), related t statistics and exact corrected p values (two tailed) at the electrode level were extracted.

2.7.3.5. N110 in cbTEP and N100 in AEP. A lateralized, negative peak around 110 ms (N110) was identified in the RCS and LCS conditions (see Result and Fig. 7J). Despite topographical differences, the comparison between RcbTEP and AEP using the ToI approach did not result in statistically significant differences (see Result and Fig. 7L), since a vertex negativity around 100 ms was recorded in the condition of auditory stimulation as well (N100). This result seems at odds with the removal of the components related to the AEPs performed to obtain RcbTEP and might indicate that the ICA failed to attenuate the N100 from AEP effectively or the nature of the two waves was different. For the former, the effectivity of reduce N100 by removing the AEP component in ICA would be examined by RcbTEP_AEP vs RcbTEP and LcbTEP_AEP

Table 2
ToIs for each comparison (see text and Fig. 2 for details).

Fig\ToI	ToI 1	ToI 2	ToI 3	ToI 4	ToI 5	ToI 6
Fig. 2A	14–20 ms	20–37 ms	37–66 ms	66–91 ms	91–132 ms	132–247 ms
Fig. 2B	14–21 ms	21–35 ms	35–60 ms	60–91 ms	91–130 ms	130–246 ms
Fig. 2C	13–25 ms	25–36 ms	36–64 ms	64–92 ms	92–131 ms	131–247 ms
Fig. 2D	13–20 ms	20–36 ms	36–64 ms	64–93 ms	93–135 ms	135–240 ms
Fig. 2E	15–21 ms	21–37 ms	37–61 ms	61–92 ms	92–132 ms	132–250 ms
Fig. 2F	13–20 ms	20–36 ms	36–69 ms	69–91 ms	91–135 ms	135–242 ms
Fig. 2G	13–21 ms	21–35 ms	35–61 ms	61–91 ms	91–133 ms	133–237 ms
Fig. 2H	13–21 ms	21–35 ms	35–60 ms	60–92 ms	92–133 ms	133–240 ms
Fig. 2I	15–22 ms	22–36 ms	36–61 ms	61–93 ms	93–140 ms	140–239 ms

vs LcbTEP. For the latter, we applied one paired comparison to test the latencies of the peak in each condition, and another procedure used previously to investigate similarity between signals of interest, with the assumption that physiologically distinct components would not show any intra-subject agreement (Rocchi et al., 2021). First, in the test for latencies, to further investigate differences between the two negative components peaking around 100 ms, we extracted the latency from the electrode having the maximal negative amplitude in each condition in ToI5. Thus, the electrodes chosen were F1 in RcbTEP and FCz in AEP. A paired comparison was performed to compare their latency. Second, we calculated the concordance correlation coefficient (CCC) to investigate possible similarities between the N110 of RcbTEP and N100 of AEP in experiment 2 (Mancuso et al., 2021; Rocchi et al., 2021), it is a form of intraclass correlation coefficient optimized to examine agreement between the distribution of two variables. It was calculated by the formula below:

$$CCC = \frac{2\sigma_{12}}{\sigma_1^2 + \sigma_2^2 + (\mu_1 - \mu_2)^2} \quad (2)$$

Here σ_{12} indicates the covariance between two distributions, σ_x^2 is the variance of distribution x, and μ_x is the average of distribution x (Kerwin et al., 2018; King et al., 2007; Lin, 1989). First, we calculated the z value of each signal (AEP and RcbTEP) in ToI5 (91–133 ms) and in a baseline window (−950 to −100 ms before TMS) separately. Next, in each electrode and in each subject, CCC was calculated between baseline and ToI5 from the two sessions, resulting in CCC between baseline ($CCC_{baseline}$) from AEP and RcbTEP and CCC between ToI5 (CCC_{ToI5}) from AEP and RcbTEP. Finally, CCC_{ToI5} was compared to $CCC_{baseline}$ with dependent samples t-test. Correction for multiple comparisons was performed by false discovery rate (FDR) (Benjamini and Hochberg, 1995). The critical value (p-value) of 0.05 or less was considered as significant in all the above statistical analyses.

2.7.4. Behavioural task

Angular error was the primary outcome measure and was calculated by measuring the angular difference between the center of the target and the line connecting the starting position to the endpoint hand position. Epochs of angular error were created by binning 8 consecutive trials. For each block, the initial mean error ($error_{int}$) was determined by averaging over the second to sixth consecutive epochs, as in previous papers, in order to sample the fast learning phase observed during adaptation (Galea et al., 2011; Krakauer et al., 2005). Large angular errors (over 60 degress) were considered outliers and rejected (1.6% of all trials) (Galea et al., 2015; Schlerf et al., 2015). To assess motor learning, a one-way repeated measure ANOVA (RM-ANOVA) was arranged to compare $error_{int}$ across baseline training ($error_{baseline\ training}$), adaptation ($error_{adaptation}$), and no vision ($error_{no\ vision}$).

Spearman's correlation coefficient were employed to measure the relationship between the change in RcbTEP amplitudes and the change in learning (de Winter et al., 2016). To calculate the change in RcbTEPs relative to different stages of the task, we measured the amplitude changes of each channel between PostBase and PreBase

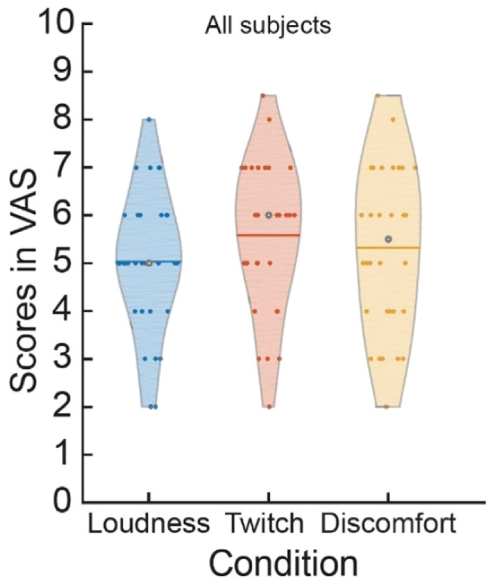

Fig. 3. All participants' VAS for RCS. Three violin plots represent the VAS for loudness (blue), twitch intensity (orange) and discomfort (yellow) by real cerebellar TMS from all 32 participants in experiment 1 and 4 (For interpretation of the references to color in this figure legend, the reader is referred to the web version of this article.)

(i.e., $RcbTEP_{Postbase\text{-}Prebase}$), and between PostAd and PostBase (i.e., $RcbTEP_{Postad\text{-}Postbase}$). To quantify the amount of fast phase learning and initial retention relative to baseline, we calculated the change of error between baseline training and adaptation (i.e., $error_{change1}$) and between baseline training and no vision (i.e., $error_{change2}$), respectively (Spampinato et al., 2017). The time windows for the above correlations were the ToIs with isolated RcbTEPs in experiment 4. In each pair, the rho value of Spearman's correlation in each channel at every ms in the ToIs were calculated by using the Fieldtrip toolbox in MATLAB. Monte Carlo permutation statistics was applied for these the spatio-temporal distribution of rho values during each ToI (channel x time) for spatial clusters and time clusters. The minimal number of neighboring electrodes for cluster-based multiple comparison was one. Other details in permutation statistics are the same as the method of statistics for cbTEPs and sensory input conditions (see above).

3. Results

3.1. Safety and discomfort

All participants tolerated the experiments and there were no dropouts nor adverse events.

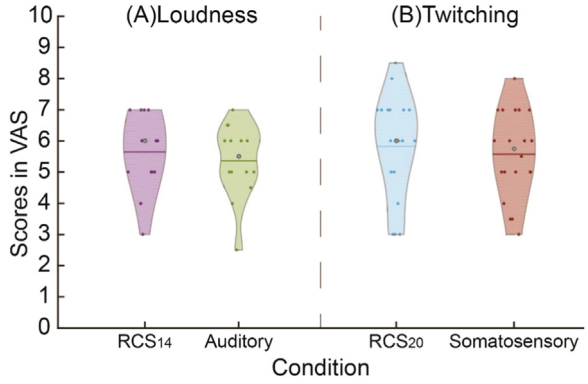

Fig. 4. VAS in each comparison. In the left panel with two violine plots, 'RCS_{14}' indicates the VAS of 14 subjects' loudness scores in RCS in experiment 1 (purple). 'Auditory' indicates is the loudness scores in auditory stimulation of experiment 2 (green). There is no difference on VAS of loudness between RCS and auditory stimulation(A). In the right panel with two plots, 'RCS_{20}' indicates 20 subjects' muscle twitching scores in RCS in experiment 1 (cyan). 'Somatosensory' refers to the scores of muscle twitching in somatosensory stimulation of experiment 3 (carmine). There is no difference on muscle twitching between RCS and somatosensory stimulation(B). Small dots indicate the individual's score. The horizontal line in each plot means the mean of the score in each condition. The gray dot is the median of the score in each condition (For interpretation of the references to color in this figure legend, the reader is referred to the web version of this article.)

3.2. Analysis of VAS

As an indication of the overall 32 participants' experience in experiments 1 and 4, the VAS for loudness was 5.03 ± 1.45, for twitch intensity it was 5.58 ± 1.55, and for discomfort it was 5.33 ± 1.70 after real cerebellar TMS (Fig. 3). The average discomfort VAS in the present study is higher than reported by Fernandez et al. (4.45 ± 1.42) (Fernandez et al., 2021), possibly because of our higher stimulus intensity. The highest discomfort score was 8.5 (only one participant with 75% MSO for RCS).

The comparisons of VAS for loudness and twitch are plotted in Fig. 4. There was no significant difference in the perception of loudness between real RCS and auditory stimulation (14 subjects: t=1.963, df=13, p=0.071) nor between RCS and somatosensory stimulation (muscle twitch) (20 subjects: t=1.648, df=19, p=0.116).

3.3. Data processing

Details of the number of removed trials, channels and components during EEG pre-processing are listed in Table 3.

Table 3
For each recording condition, the table lists the number of trials removed ("Trials"), the number of electrodes interpolated ("Electrodes") and the number of independent components removed in each round of ICA ("ICA1" and "ICA2" for the first and second round, respectively). Values are expressed as mean ± standard deviation. "Auditory" indicates auditory stimulation. "Somatosensory" refers to somatosensory stimulation.

Conditions	Trials	Electrodes	ICA1	ICA2
Experiments 1–3				
RCS	12.6 ± 9.1	0.5 ± 0.7	7.0 ± 2.8	35.6 ± 5.6
LCS	10.6 ± 10.8	0.6 ± 0.8	7.8 ± 2.4	34.5 ± 5.1
Auditory	4.2 ± 5.3	0.1 ± 0.3	2.7 ± 1.3	30.8 ± 6.0
Somatosensory	7.2 ± 9.8	0.1 ± 0.3	4.3 ± 2.3	37.1 ± 5.2
Experiment 4				
PreBase	10.4 ± 9.9	0.4 ± 0.7	8.1 ± 2.1	30.9 ± 7.1
PostBase	3.4 ± 3.4	0.1 ± 0.3	6.9 ± 3.4	34.6 ± 7.2
PostAd	6.3 ± 5.9	0.4 ± 0.5	8.0 ± 3.0	29.8 ± 6.6

3.4. CBI measurement on MEP

In experiment 1, the intensity of LM1-TS was 71.7 ± 13.3% MSO and the intensity of RM1-TS was 71.9 ± 12.5% MSO. In experiment 4, the intensity of LM1-TS was 65.7 ± 10.6% MSO. All cerebellar intensities have been listed in Table 1. MEPs were suppressed in all CBI conditions (Fig. 5A–C). This was true in experiment 1 for both LM1-TS vs L-CBI (1.28 ± 0.51 mV vs. 1.10 ± 0.50 mV, z = −3.889, p < 0.001) and RM1-TS vs R-CBI (1.53 ± 0.64 vs. 1.42 ± 0.60 mV, z = −3.527, p < 0.001). The CBI ratio of L-CBI was 0.86 ± 0.14 and for R-CBI was 0.93 ± 0.08. A similar inhibition occurred in experiment 4 when comparing LM1-TS and L-CBI (1.42 ± 0.45 mV vs. 1.14 ± 0.42 mV, t= −3.920, df=13, p = 0.002). These results indicate that the intensity and scalp location of cerebellar stimulation could generate adequate output to the cerebral cortex. Fig. 5D illustrates the CBI ratio and the corresponding intensity of cerebellar stimulation for each participant in experiment 1 (both sides) and experiment 4 LCBI only). Intensities above 70% MSO provide stable inhibition.

3.5. Characterisation of cbTEPs evoked by single-pulse cerebellar stimulation

Fig. 2 illustrates the ToIs used in each set of experiments. These were estimated from the GMFP averages, which are also summarized in Table 2. Moreover, Table 4 summarises all statistical values obtained in cbTEP pairwise comparisons.

3.6. Resting TMS-EEG responses without removal of AEP components

Because of the strong auditory and somatosensory input produced by cerebellar stimulation, signals generated in RcbTEP_AEP, LcbTEP_AEP and AEP conditions share obvious similarities in ToIs 5 and 6, where their topography is dominated by a vertex N100 and P200 (Fig. 6A–C). Similar potentials around the vertex are also presented in the somatosensory stimulation condition, albeit with a smaller amplitude (Fig. 6D). However, there appear to be differences in earlier ToIs, as confirmed by pairwise comparisons. Both RcbTEP_AEP and LcbTEP_AEP elicited two contralateral frontal waves, one positive (P80) in ToI4 and one negative (N110) in ToI5; due to this lateralization, pairwise comparisons led to statistically significant differences between them (Fig. 6G). The differences were bilateral over ToI5, as expected from a symmetrical mirrored N110. However, statistical differences only occurred in the left hemisphere in ToI4, suggesting that the P80 might have been smaller after LCS. This will be discussed further in later sections. Cerebellar stimulation also elicited an earlier ipsilateral parietal negative wave in ToI1, again leading to a statistically significant bilateral difference between RcbTEP_AEP and LcbTEP_AEP (Fig. 6G).

The P80 in ToI4 in RcbTEP_AEP was absent in both the AEP and SEP conditions, replaced by central negativity (Fig. 6H–K). Additional differences between RcbTEP_AEP and SEP were present in ToI1 due to the ipsilateral parietal negative component induced by RcbTEP_AEP and in ToI5, where the lateralized RcbTEP_AEP N110 and the SEP vertex N100 appeared (Fig. 6K).

3.7. Resting TMS-EEG responses after removal of AEP components by means of ICA

After ICA processing, the prominent central N100/P200 waves in ToI5 and ToI6 of RcbTEP_AEP and LcbTEP_AEP conditions were, as expected, reduced (Fig. 7A–D). The pairwise comparisons in Fig. 7E–H indicate where processing had the greatest effects on the potential distributions in the topoplots. In addition, they also demonstrate that the ICA processing did not significantly affect the signals in ToI1-ToI4.

Pairwise comparisons between stimulation conditions yielded results similar to those obtained prior to the removal of AEP components (Fig. 7), but with some small differences. While the differences remained

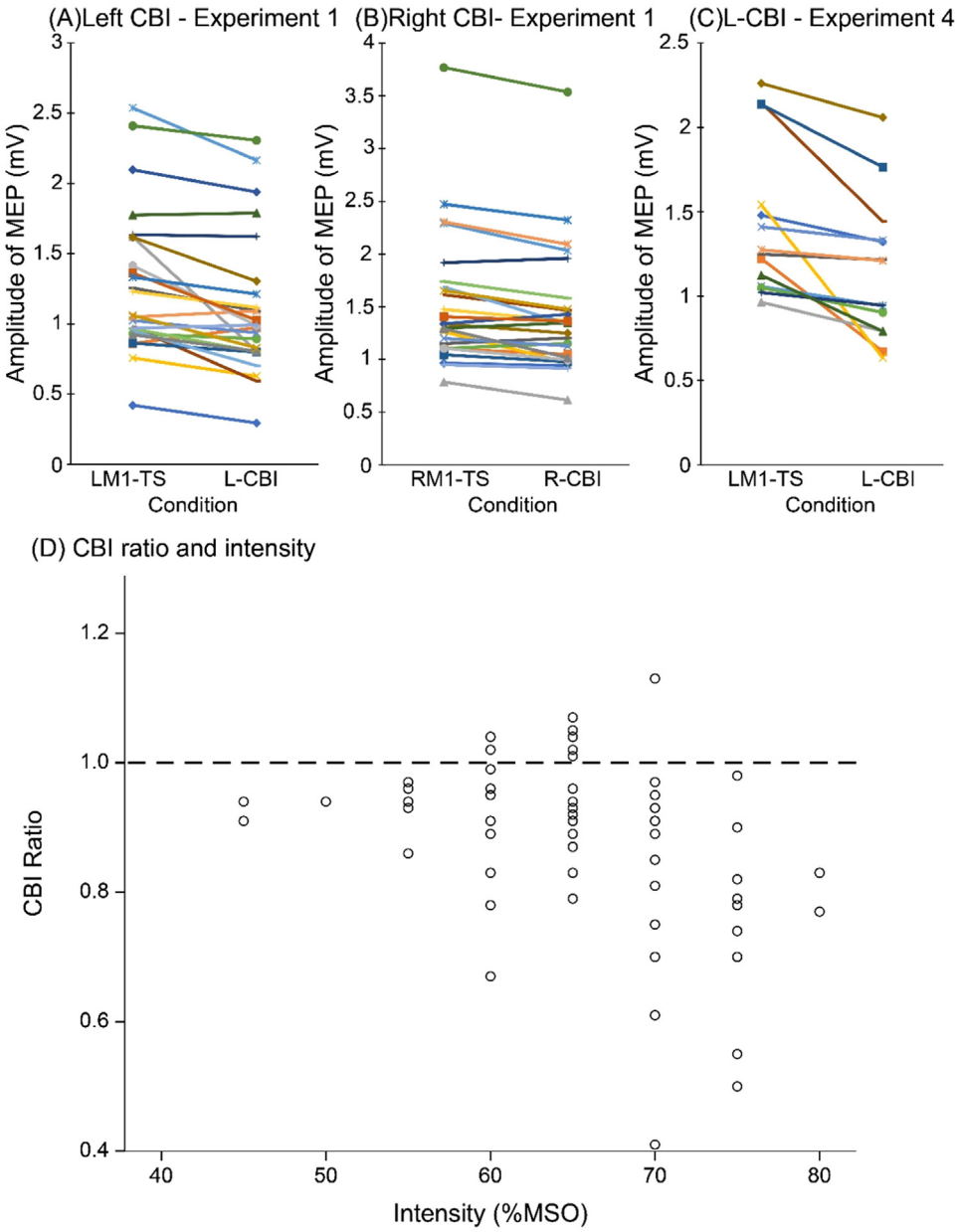

Fig. 5. Cerebellar-brain inhibition assessed by MEPs. The upper panel displays the change of amplitude of MEPs in each block (A–C). The bottom panel shows all CBI values in this study, including both sides CBI in experiment 1 and left CBI in experiment 4 (D).

at ToI1 and ToI5 in the comparison of RcbTEP and LcbTEP, removal of the AEP now showed that the comparison of P80 in ToI4 was significant bilaterally, rather than solely on the left (Fig. 7J compare Fig 6G). The comparison between RcbTEP and AEP confirmed the difference in ToI4, but there was also a significant negative cluster at the vertex site in ToI6, due to the attenuation of P200 (Fig. 7L). The differences between RcbTEP and SEP observed in ToIs1, 4 and 5 (Fig. 6K), were maintained (Fig. 7N), but there was no difference in ToI6 even after attenuating the P200.

The lateralisation of the N110 after cerebellar stimulation is consistent with the side of cerebellar stimulation, so it was surprising that there was no statistical difference in ToI5 between RcbTEP (or RcbTEP_AEP) and AEP (Figs. 6I and 7L). We suspected this was due to the close spatial overlap of a cerebellar N110 and a sensory N100. Indeed, there was a significant difference in latency of the N110 after RCS and the N100 after auditory stimulation (108.2 ± 6.9 ms vs 91.9 ± 10.4 ms, z=−3.173, p=0.002) (Fig. 8A). The CCC analysis performed to investigate possible similarities between RcbTEP N110 and AEP N100 did not yield significant results (Fig. 8B), consistent with, although not proof of the idea that they may represent different cortical evoked potentials.

In sum, these data suggest that, although much of the evoked EEG activity produced by TMS over the lateral cerebellum is due to sensory input, a significant frontal positive/negative potential in ToI4/ToI5 may result from activity in cerebello-cortical projections (a cbTEP). In the second half of the paper, we probed this hypothesis by asking if the amplitude of the cbTEP would be sensitive to state-dependent changes in cerebellar activation that occur during visuomotor adaptation in an arm-reaching task. The analysis of EEG signals is confined to ICA-processed data to remove the AEP.

3.8. Analysis of angular error during visuomotor adaptation

In the baseline training, the mean angular error was −1.9 ± 1.55°. Following introduction of the visual rotation, the mean angular error increased to −9.6 ± 2.9°. After removing both visual rotation and the visual cursor, participants had a clockwise mean angular error of 13.6 ± 2.9°(Fig. 9). There was a significant difference in learning over the

Table 4
Summary of statistically significant differences obtained in pairwise comparisons of TEPs (see text for details).

Comparisons	Figure	Cluster	TOI1	TOI4	TOI5	TOI6
Rest state (Experiment 1–3)						
RcbTEP_AEP vs LcbTEP_AEP	Fig. 6G	Positive	p=0.018	p=0.023	p=0.026	–
		Negative	p=0.005	–	p=0.022	–
RcbTEP_AEP vs AEP	Fig. 6I	Positive	–	p<0.001	–	–
		Negative	–	p<0.001	–	–
RcbTEP_AEP vs SEP	Fig. 6K	Positive	p=0.006	p<0.001	–	–
		Negative	p=0.004	p<0.001	p=0.024	–
RcbTEP_AEP vs RcbTEP	Fig. 7F	Positive	–	–	–	p=0.002
		Negative	–	–	p=0.003	p=0.025
LcbTEP_AEP vs LcbTEP	Fig. 7H	Positive	–	–	–	p=0.013
		Negative	–	–	p=0.030	p=0.004
RcbTEP vs LcbTEP	Fig. 7J	Positive	p=0.008	p=0.022	p=0.013	–
		Negative	p=0.027	p=0.005	p=0.030	–
RcbTEP vs AEP	Fig. 7L	Positive	–	p<0.001	–	p=0.015
		Negative	–	p<0.001	–	p=0.002
RcbTEP vs SEP	Fig. 7N	Positive	p=0.026	p<0.001	–	–
		Negative	p=0.035	p<0.001	p=0.042	–
Visuomotor adaptation (Experiment 4)						
PreBase vs PostBase	Fig. 10G	Positive	–	p<0.001	p=0.014	–
		Negative	–	–	p=0.003	–
PostBase vs PostAd	Fig. 10H	Positive	–	–	–	–
		Negative	–	p=0.004	–	–
PreBase vs PostAd	Fig. 10I	Positive	–	–	p=0.004	–
		Negative	–	–	p=0.002	–
Spearman's correlation	Fig. 10J	Positive		p=0.037 (66–93 ms)	–	
		Negative		p=0.030 (62–80 ms)	–	

three blocks ($F_{2,26}$=224.143, p<0.001). Post hoc significant comparisons were: $error_{baseline\ training}$ vs $error_{adaptation}$ (p<0.001); $error_{adaptation}$ vs $error_{no\ vision}$ (p<0.001); $error_{baseline\ training}$ vs $error_{no\ vision}$ (p<0.001).

3.9. Cerebellar TMS-EEG responses during visuomotor adaptation

The averaged topographies of PreBase RcbTEPs in experiment 4 were similar to those RcbTEPs in experiment 1 (Fig. 10A and D). The comparison between PreBase and PostBase RcbTEPs revealed that, after baseline training, the left frontal positive peak at ToI4 (P80) was significantly suppressed (Fig. 10G, note that positive t value is PreBase - PostBase); the amplitude of this positive cluster was restored to baseline levels after the adaptation block (Fig. 10H and I). Changes in the negative deflection (N110) in ToI5 had a different time course: while it was suppressed at PostBase (Fig. 10G), it remained suppressed for the whole duration of the task (Fig. 10H and I).

We also explored potential relationships between motor learning and changes in amplitude of RcbTEPs. There was a significant positive correlation (Spearman non-parametric) between the amount of retention ($error_{change2}$) and $RcbTEP_{Postad\text{-}Postbase}$ of a large frontal-parietal network at P80 (Fig. 10J): the greater the retention, the more significant the change in amplitude of the P80 (Fig. 11). But there was no correlation between N110 and $error_{change1}$ or $error_{change2}$.

4. Discussion

Our results demonstrate that interactions between the cerebellum and cortex can be evaluated using TMS-EEG and that these change during motor learning. We argue that these results provide a neurophysiological read-out of cerebellar inputs that are processed by the cortex and are related to visuomotor learning.

4.1. Cerebellar TMS evoked potential (cbTEP) can be recorded with TMS-EEG

The goal of experiments 1–3, performed in resting state, was to determine whether it was possible to identify a cortical EEG response that was due to activity in cerebellar-cortical connections and that was separate from potentials evoked by auditory and somatosensory stimulation caused by discharge of the TMS coil. Separate control conditions were used to identify activity produced by auditory and somatosensory input since previous work has shown that the EEG produced by each summates linearly and, therefore, it is not necessary to devise a single control condition that combines both sensations (Rocchi et al., 2021). We argue that comparing across all conditions (RcbTEP_AEP, LcbTEP_AEP, AEP, and SEP; Fig. 6) provides sufficient evidence to disentangle sensory "EEG activity" from responses due to input from the cerebellum. Of note, all conditions have large potentials in ToI5 and ToI6 (see butterfly plots, approximately around 90–130 ms and 130–250 ms) that correspond to sensory-induced vertex N100 and P200 peaks (see topographic plots) (Mouraux and Iannetti, 2009), a result that has been previously described in TMS-EEG studies (Gordon et al., 2021; Rogasch et al., 2014). The auditory stimulation and somatosensory stimulation conditions, which activate auditory and somatosensory pathways, additionally showed a negative vertex potential at ToI4 (around 60–90 ms) similar to that described by others using a multisensory control condition (Fernandez et al., 2021; Sasaki et al., 2022), which was not seen when stimulation was given to the cerebellum.

In ToI4, RcbTEP_AEP and LcbTEP_AEP conditions were characterised by a contralateral positive peak (P80) over frontal cortex consistent with activation of cerebellar-cortical connections (Middleton and Strick, 2001; Strick et al., 2009; Watson et al., 2014), together with an occipital negativity, which could mask the early central negative potential from SEP and AEP. Lateralized activity is also seen at ToI1 and ToI5 (Fig. 6E–G). While speculative, the differences at ToI1 (around 13–20 ms) are likely due to initial artefacts caused by the TMS coil activation (Fig. 6I) ipsilateral to the side of stimulation. It is more challenging to make a definite conclusion about the cause of the lateralised N110 produced by RcbTEP_AEP at ToI5 since it overlaps with the auditory vertex negativity that occurs at a similar timing (see comparison of RcbTEP_AEP with AEP in Fig. 6I).

Similar conclusions were reached after ICA processing, which attenuated the N100 and P200 significantly (Fig. 7E–H) without affecting earlier components. There was a clear contralateral frontal positivity at ToI4 and a contralateral negativity at ToI5 (Fig. 7B, D and J), the latter

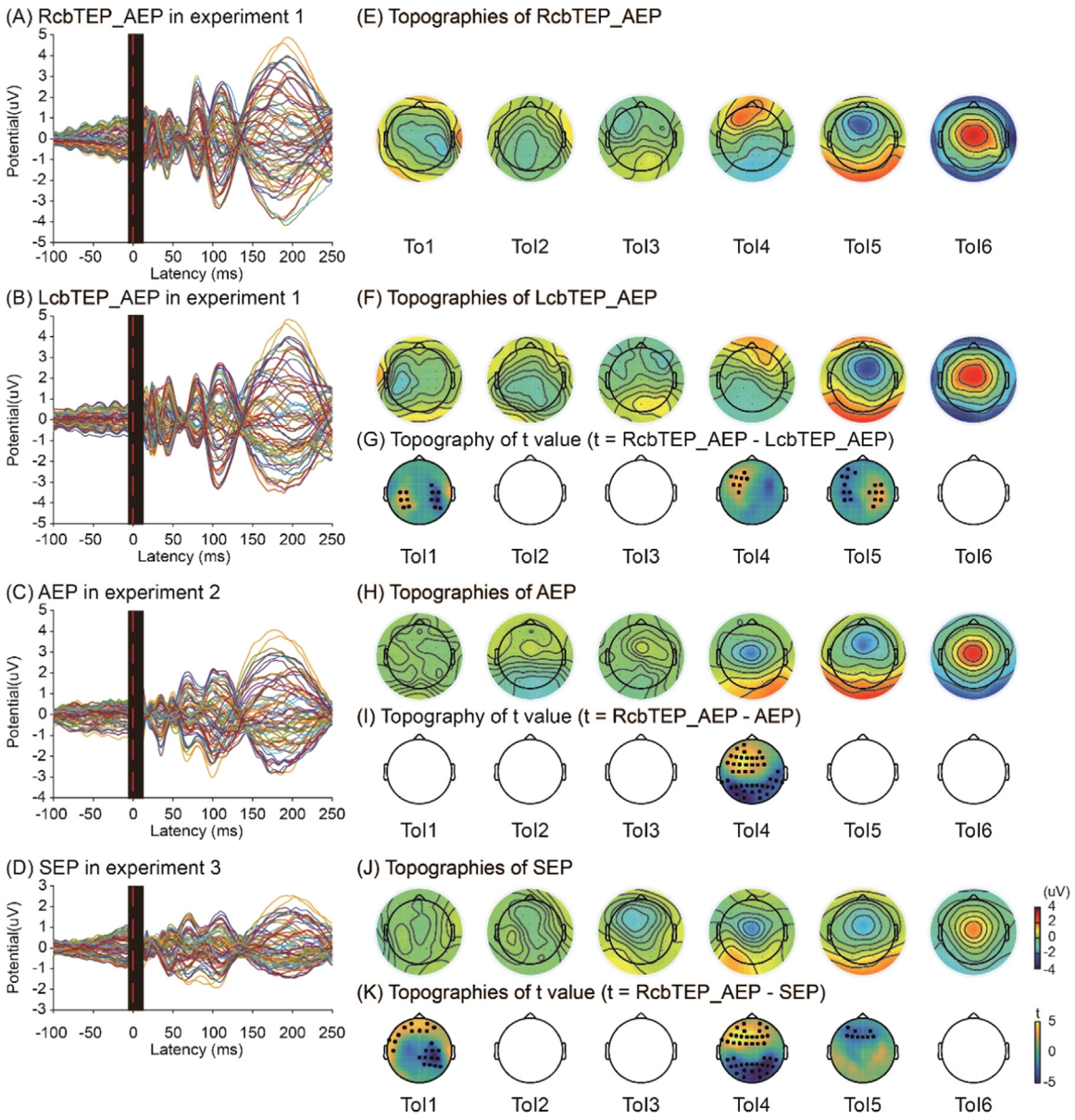

Fig. 6. Descriptive summary and statistics of cbTEPs keeping AEP and sham controls from resting state experiments. Left panels illustrates the grand average butterfly plots of 25 subjects' RcbTEP_AEP (A), 25 subjects' LcbTEP_AEP (B), 14 subjects' AEP (C) and 20 subjects' SEP (D) conditions. The red dashed line is the time point of TMS pulse. The black panel around the TMS pulse is the time window which was cut to remove the TMS pulse artefact where the TMS pulse artefact (−5 to 12 ms). The right panels show scalp topographies and t value maps for each paired comparison, referring to the same conditions of left panels: 25 subjects' RcbTEP_AEP topographies (E), 25 subjects' LcbTEP_AEP topographies (F), t values map of RcbTEP_AEP vs. LcbTEP_AEP (G), 14 subjects' topographies of brain response to AEP (H), t values map of RcbTEP_AEP vs. AEP (I), 20 subjects' topographies of brain activity evoked by SEP (J), and t values map of RcbTEP_AEP vs. SEP (K). In the t value maps, black dots indicate significant electrodes by cluster based permutation test (For interpretation of the references to color in this figure legend, the reader is referred to the web version of this article.)

being more difficult to interpret. Some pieces of evidence seem indicate the existence of a N110 produced by cerebellar stimulation. These are the significant difference between RcbTEP and SEP in ToI5 (Fig. 7N), the difference in latency (Fig. 8A) and lack of similarity (Fig. 8B) between the N110 and AEP N100, and the significant lateralisation (Fig. 7J) and modulation of the N110 by the behavioural task (Fig. 10G and I). However, even after AEP suppression by ICA, the comparison between cbTEP and AEP failed to show a difference in ToI5, indicating that the spatiotemporal distribution of the lateralised N110 could not be separated from the AEP N100 (Fig. 7L). Additionally, despite the observed changes, there was no correlation between the angular error and the N110 amplitude. Based on this evidence, it is possible that the N110 represents a mixed signal generated by both cerebellar and auditory stimulation.

Regarding the residual P200 that persists after ICA processing, although RcbTEP and AEP differ in ToI 6 (Fig. 7L), there is no difference between RcbTEP and SEP in the same ToI (Fig. 7N). In addition, this residual P200 is not modulated by the visuomotor learning (Fig. 10), suggesting that it could at least partly reflect a vertex potential. Thus we cannot exclude the possibility that it results from an incomplete suppression of the sensory P200, as in a previous study (Ross et al., 2022).

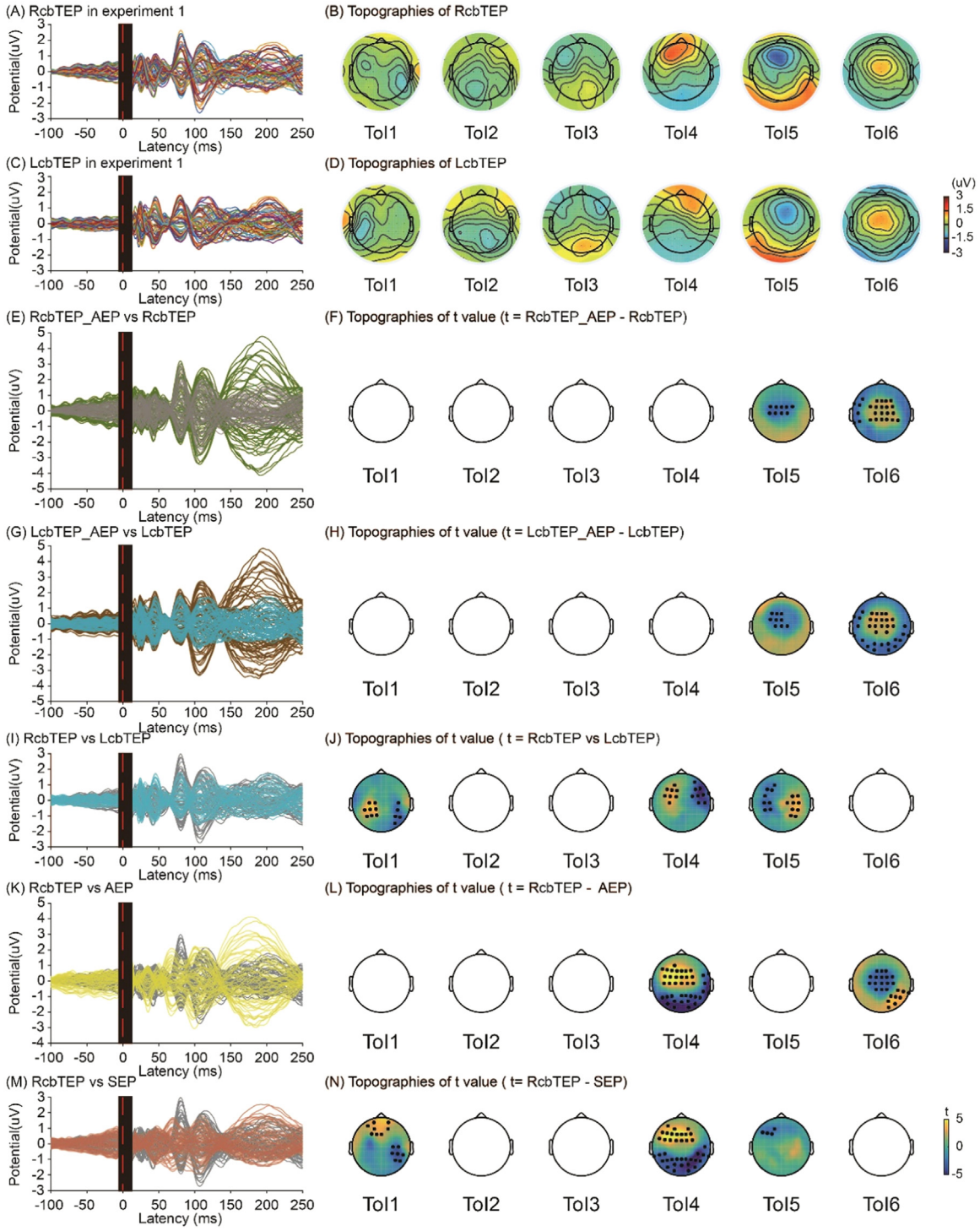

Fig. 7. Descriptive summary and statistics of cbTEPs from resting state experiments. Grand average butterfly plot (A) and topographies (B) of 25 subjects' RcbTEP. Grand average butterfly plot (C) and topographies (D) of 25 subjects' LcbTEP. From third row below, left panels show the overlapped butterfly plots for each comparison, and the right panels indicate the t value maps for each comparison. In the left panels, the gray butterfly plot is always RcbTEP, and the blue one is always LcbTEP. When comparing RcbTEP_AEP vs. RcbTEP, a clear vertex N100 and P200 peaks are present in the green butterfly plot of RcbTEP_AEP (E) and in the t value maps of ToI5 and ToI6 (F). LcbTEP_AEP vs. LcbTEP comparison showed similar results (G, H). The comparison between RCS and LCS conditions (I) showed significant clusters in ToI1, ToI4 and ToI5, consistent with contralateral cortical activation following cerebellar stimulation (J). In the RcbTEP vs. AEP comparison (K, L), the larger vertex P200 of the latter resulted in a central significant negative cluster in ToI6, while a lateralized frontal P80 in the RCS condition resulted in a significant positive cluster in ToI4, but a peak of RcbTEP in middle latency has higher amplitude than AEP (K). In the last row, RcbTEP vs. SEP comparison (M, N) demonstrates a very early peak in ToI1, another high peak in ToI4 and the other clear negative peak in ToI5 in butterfly plot of RcbTEP (M), referring to the significance in t value maps (N). The red dashed line is the time point of TMS pulse. The black panel around the TMS pulse is the time window which was cut to remove the TMS pulse artefact where the TMS pulse artefact (−5 to 12 ms). In the t value maps, black dots indicate significant electrodes by cluster based permutation test (For interpretation of the references to color in this figure legend, the reader is referred to the web version of this article.)

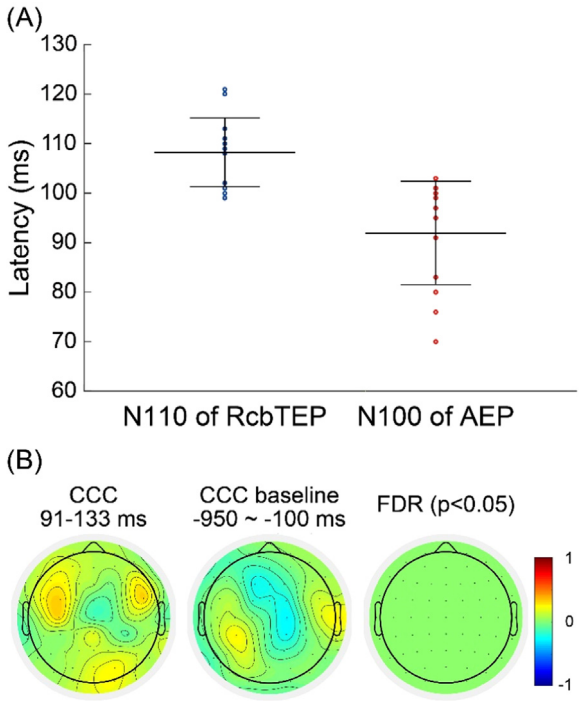

Fig. 8. Latency comparison and concordance correlation coefficient calculation of N100 and N110 waves. The top panel demonstrates the difference in latency between N110 of RcbTEP and N100 of AEP (A). The bottom panel shows the CCC between RcbTEP and AEP in ToI5 (91–133 ms) (left) and in a baseline window (−950 ms to −100 ms, middle); the right plot shows not significant CCC values (B).

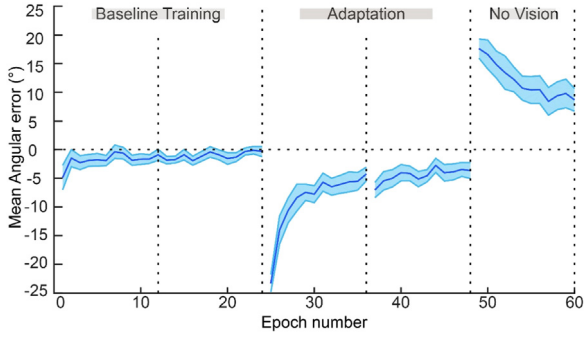

Fig. 9. The learning curve of behavior tasks. The learning curve of experiment 4 is represented. Blue shaded area indicates the 95% confidence interval of angular error (For interpretation of the references to color in this figure legend, the reader is referred to the web version of this article.)

4.2. cbTEPs are modulated by visuomotor learning

As visuomotor learning is well-known to engage cerebellar interactions with both motor and cognitive cortical areas (Galea et al., 2015, 2011; Halsband and Lange, 2006; Spampinato and Celnik, 2021; Spampinato et al., 2017; Taylor and Ivry, 2014), we expected changes in the cbTEP to appear throughout frontal-motor areas following learning. We did not expect changes surrounding the occipital lobe, as previous work has shown that this area does not involve this area during cerebellar visuomotor adaptation (Boukrina and Chen, 2021; Haar et al., 2015; Striemer et al., 2019). Our data demonstrated that the frontal P80 was sensitive to different stages of training (Fig. 10). A decrease in this peak was found following task familiarization, which subsequently increased following adaptation. Interestingly, we found that changes in the P80 peak correlated to the amount of motor retention, indicating that this peak is an important marker for learning. While we additionally found that the N110 peak was modulated following baseline performance, we found no behavioural correlations associated with this peak, hinting that P80 and N110 provide information about different processes that may be more or less directly related to motor learning and retention (Fig. 10J).

The fact that cbTEP changes were concentrated over prefrontal areas might not be surprising as the most likely cerebellar zones stimulated with TMS are ones associated with cognition (i.e., lobules VI to Crus I/II) (Bernard and Seidler, 2013; Krienen and Buckner, 2009; Strick et al., 2009). Additionally, adaptation to visuomotor rotations requires different forms of learning that are associated with distinct neural substrates, such as learning *via* sensory prediction errors that are calculated by the cerebellum and cognitive strategies (i.e., aiming) that involve frontal areas (Taylor and Ivry, 2014; Tzvi et al., 2020). As the P80 changes were concentrated in contralateral prefrontal areas following cerebellar visuomotor adaptation, they may reflect long-term depression of Purkinje cells and increased activity across the cerebellar-prefrontal network (Shadmehr and Holcomb, 1997) as, collectively, these regions play an important role in learning and consolidating new sensorimotor transformations (Caligiore et al., 2019; Tzvi et al., 2020). This is supported by evidence that the strength of connectivity in the cerebellar-cortical network updates dynamically after learning is completed, during consolidation and automatization (Doyon et al., 2009) and also during processes involving motor memory formation (Bedard and Sanes, 2011). In line with this, the P80 may reflect the overall state of the cerebellar-prefrontal pathway at different stages of visuomotor adaptation rather than a cerebellar state or prefrontal state alone.

Previous MRI studies have pointed out that the cerebellum and prefrontal cortex are engaged throughout visuomotor adaptation learning. Activation of both areas are seen at the initial stages of adaptation (Shadmehr and Holcomb, 1997; Tzvi et al., 2020), while the right anterior cerebellar and left premotor activity persist for several hours after individuals have adapted their movements during a consolidation period (Shadmehr and Holcomb, 1997). This may explain why the change in P80 outlasts the period of learning and is related to a specific aspect of visuomotor learning. Indeed, the modulation of the P80 peak following adaptation was strongly correlated with the amount of displacement observed in no vision trials. These trials, where no rotation or vision of the cursor was administered, were used to assess how much of the new reaching pattern has been stored following adaptation. Here, individuals who displayed more errors (an indicator of more retention) during these trials also had significantly larger changes in P80 peaks with respect to baseline (Figs. 10J and 11) .

One question here is, why do the amplitudes of P80 and N110 fluctuate after baseline training as well as adaptation? We speculate that these data might reflect some aspects of initial learning that are driven by cognitive processes, such as aiming and tool learning (Nezafat et al., 2001). Indeed, participants initially showed a bias in their goal-directed reaches, which were found to reduce with repetitive training as they learned to use the manipulandum. Future work may consider probing changes in the cbTEP before and after simple reaching movement alone (i.e., without manipulandum), which avoids any learning effects.

4.3. Comparison with previous studies of cbTEPs

As noted in the introduction, results are not consistent across studies and there are substantial differences in the methodology used (e.g. TMS coil type, intensity, and stimulation site). However, it is interesting to note that the study by Sasaki et al. which used a DC coil as in the present experiment, yielded a contralateral frontal positivity at 80 ms similar to that described here. However, the authors did not do a paired comparison with sham control, so the conclusion is based only on an inspection of their data (Sasaki et al., 2022). In contrast, two studies that used F8 coils do not comment on any activity specific to cerebellar stimulation around 80 ms and reported conflicting results. Using a 50 mm F8 coil, Gassmann and colleagues reported a diffuse negative contralat-

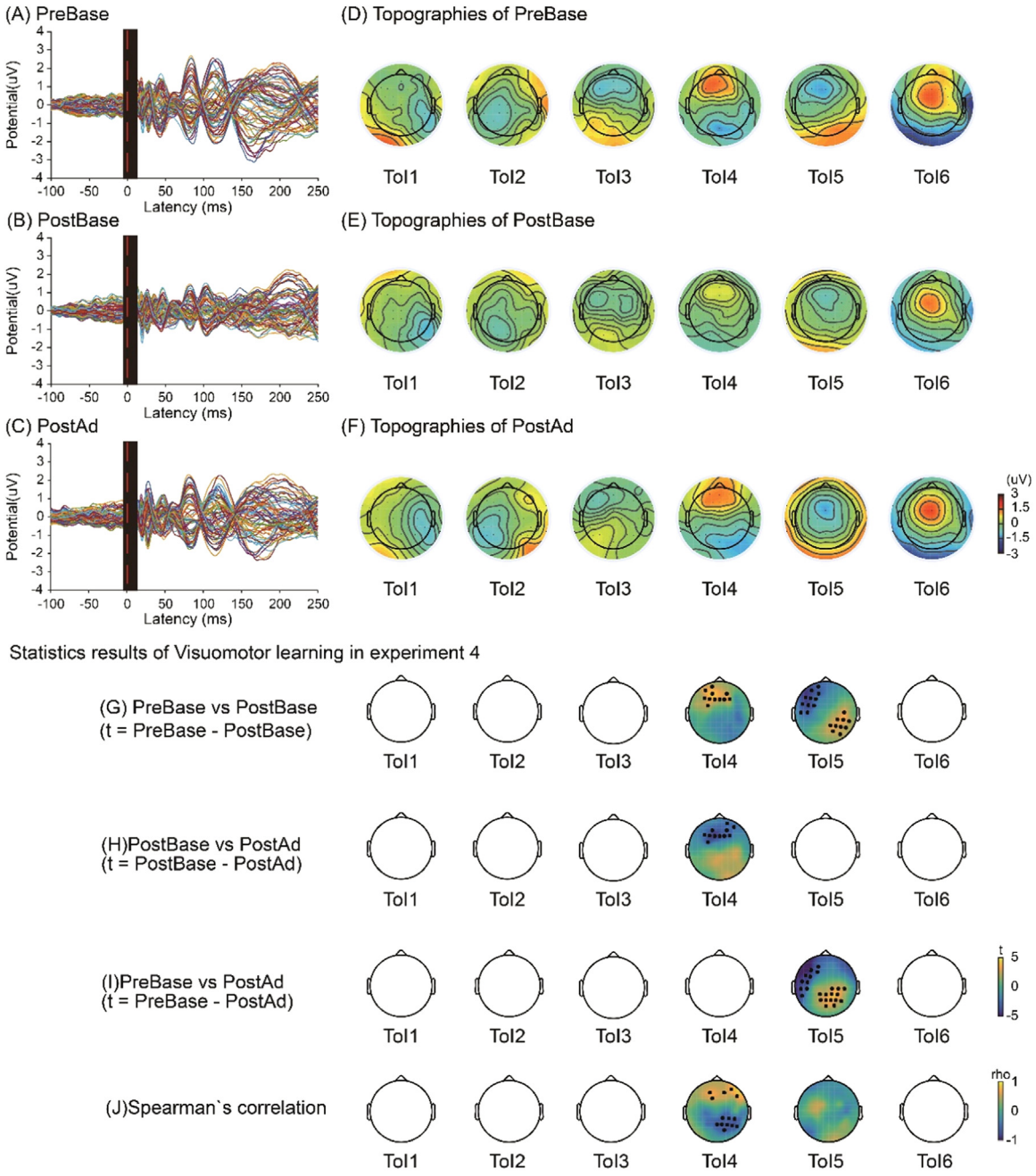

Fig. 10. Summary of statistics from experiment 4. Upper left panels show butterfly plots of RcbTEPs in PreBase (A), PostBase (B), and PostAd (C) recording blocks. The P80 and N110 amplitudes are clearly reduced in PostBase (B) and restored in PostAd (C). Upper right panels show topographies correlating to the left side: PreBase (D), PostBase (E), and PostAd (F). ToIs are based on Fig. 2I. Again, the changes in P80 (ToI4) and N110 (ToI5) on topographies (D, E, F) are the same as the butterfly plots, whereas there are no obvious changes in other ToIs. The bottom panels plot the t value maps of paired comparison in upper three rows, including PreBase vs PostBase (G), PostBase vs PostAd (H), and PreBase vs PostAd (I). In ToI4, the P80 at PreBase is significantly higher than PostBase (G), and the P80 at PostBase is significantly lower than PostAd (H). In ToI5, N110 at PreBase has more negative amplitude than PostBase and PostAd (G, I). The bottom row depicts the rho value topographies of Spearman's correlation (J). The P80 correlates to the learning performance ($error_{change2}$). The red dashed line is the time point of TMS pulse. The black panel around the TMS pulse is the time window which was cut to remove the TMS pulse artefact where the TMS pulse artefact (−5 to 12 ms). In the t and rho value maps, black dots indicate significant electrodes by cluster based permutation test (For interpretation of the references to color in this figure legend, the reader is referred to the web version of this article.)

eral potential at around 45 ms (Gassmann et al, 2022), which was not replicated by another study using a 70 mm F8 coil (Fernandez et al., 2021). It is plausible that coil type, stimulation intensity and site may account for discrepancies in results across different studies. For instance, DC coils are more effective than F8 coils in activating cerebellar projections to the cortex (Fernandez et al., 2018; Hardwick et al., 2014; Spampinato et al., 2020a). We also carefully calibrated cerebellar TMS intensity based on CBI, a procedure not performed in the paper by Fernandez and coworkers, who used a fixed intensity. It is also clear that changing the intensity of cerebellar stimulation can result in differences in CBI (Galea et al., 2009; Hardwick et al., 2014; Spampinato et al., 2020a; Ugawa et al., 1995). The stimulus intensities for the F8 coil used by Fernandez et al. (90%MSO) and Gassmann et al. (75% MSO) are quite different and thus may partially explain differences between their

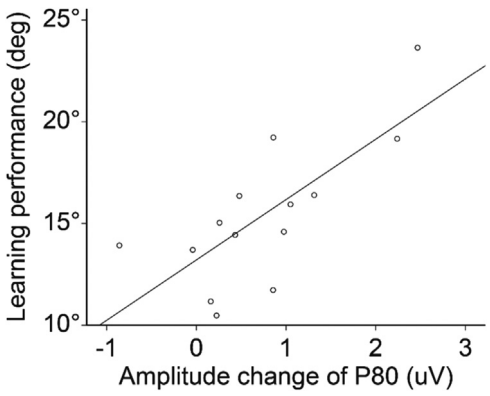

Fig. 11. Correlation between changes of P80 and learning performance. This graph depicts the relationship between learning performance ($error_{change2}$, y-axis) and the change of P80 (x-axis). The change of P80 means the averaged difference of amplitude, by PostAd subtracting PostBase, of the significant frontal cluster during the significant time window.

results. In addition, various stimulation sites across studies may also be responsible for the diverging results: whereas we stimulated 3 cm lateral to the inion, as in other studies where CBI was successfully obtained (Daskalakis et al., 2004; Fernandez et al., 2021; Fong et al., 2021; Hardwick et al., 2014; Pinto and Chen, 2001; Spampinato et al., 2021, 2020a, 2020b), Gassmann and co-workers chose a site corresponding to PO10, a site more lateral and previously reported to not suitable for eliciting CBI (Ugawa et al., 1995).

Measurement of the electrical field (E-field) induced by TMS provides a useful estimation of the effectiveness of cerebellar TMS. A study by Çan and coworkers (Çan et al., 2018) suggested that (1) lateral (i.e., PO9) and medial (i.e., I1) stimulation sites induce significantly different distribution of E-field and that (2) 110 mm DC coils provide deeper stimulation compared to F8 coils, whose stimulation is more focal but limited to the cerebellar cortex. This is important since, according to previous literature, cerebellar motor areas are located deep in lobules V and VIII, about 3–3.5 cm from the scalp (Hardwick et al., 2014). These findings agree with our E-field measurements (summarized in supplementary material 3 and Fig. S2). Overall, we conclude that a consistent method for stimulating the cerebellum should be adopted in the future and that putative cerebellar evoked potentials are shown to be behaviourally sensitive.

4.4. EEG recording reveals more details of the neurophysiology of single-pulse subthreshold cerebellum TMS with a DC coil

Cerebellar Purkinje cells are thought to be activated by TMS, which inhibits the dentate nucleus neurons that project to the cortex *via* the thalamus (Battaglia et al., 2006; Reis et al., 2008; Rossini et al., 2015). Given the large and non-focal stimulation applied with the DC coil, it is likely that cerebellar projections to the motor and cognitive areas are activated. Interestingly, the area of the cerebellar cortex closest to the scalp is the Crus I/II (~ 13–15 mm) (Benjamini and Hochberg, 1995; Galea et al., 2011), which connects to prefrontal cerebral areas (Benagiano et al., 2018; Middleton and Strick, 2001; Strick et al., 2009; Watson et al., 2014). In other words, the bulk of single pulse cerebellar TMS likely activates Purkinje cells in Crus I/II, which would suppress background firing in the dentate nucleus and transiently suppress the excitatory thalamic-frontal relay, similar to CBI. This suggests that our observed prefrontal potential (P80 and possibly part of the N110) is not due to direct activation of dentato-thalamo-cortical projections, as these would be inhibited by cerebellar stimulation, but would rather represent an excitatory rebound phenomenon of stimulating the highly active inhibitory Purkinje cells. This response is likely to be sensitive to visuomotor learning because it is clear that plastic changes are expected in both the cerebellum and prefrontal lobe, given their important contributions to learning this task (Galea et al., 2015; Halsband and Lange, 2006; Taylor and Ivry, 2014).

5. Limitations

The high intensity and DC coil used to evoke cerebellar output present a challenge, as this may lead to large evoked auditory evoked potentials. In addition, slightly vary coil position, different coil types and stimulation intensities we might be able to stimulate different projections and hence get different cbTEPs. Thus, depending on how well this aspect is controlled for, these potentials could potentially drive variable results among future cerebellar TMS-EEG studies. Moreover, studies have used different intensities of stimulation to activate the cerebellum, a problem compounded by the fact that AMT_{BS} cannot be measured in some participants. Nevertheless, we can compare the present range of intensities to the previous work of Gassmann and coworkers. They illustrated the homogeneity of their data by showing that 82.6% (38 of 46 measurements) of participants' CBI ratios fell within 1 standard deviation of the mean (Gassmann et al., 2022). In the present data, 78.1% (50 of 64 measurements) of participants' CBI ratios fell within the same range. Furthermore, the use of ICA as a method of EEG pre-processing is another potential issue because signals generated by direct brain stimulation and activation by sensory input might not be independent. However, the spatial and temporal profile of EEG responses generated by sensory input of TMS has been well characterized (Rogasch et al., 2014; Ross et al., 2022), which makes their identification and removal easier. It is also important to note that several review papers by experts on the topic exist (Hernandez-Pavon et al., 2023; Tremblay et al., 2019), and no definite recommendations on pre-processing options are provided. Nevertheless, it is important to note that, even after ICA, residual vertex activity partly remains, as reported also by Ross and colleagues (Ross et al., 2022), and may contribute to the mentioned issues in N110 and P200 interpretation. Finally, the stimulus produces a large artifact in early EEG components that cannot be filtered. Thus, it is difficult to see the earliest response known to influence M1 activity since the rebound of excitability of dentato-thalamo-cortical tract occurs within 10 ms, as demonstrated in CBI studies using EMG (Ugawa et al., 1995).

6. Conclusion

Using the DC coil and enough stimulus intensity, together with careful EEG pre-processing, the results demonstrate that a cortical response to cerebellar TMS (P80 and, at least partly, N110) can be isolated and is reproducible across different groups of subjects. Visuomotor learning influenced the amplitude of cbTEP (P80) consistent with its origin in the cerebellum. However, because of the large sensory inputs produced by cerebellar TMS, which interfere with identification of later parts of the cbTEP, further investigation of the N110 is still needed.

Data and code availability statement

The participants' details are confidential because of privacy. The analysis in the study was performed using open-sourced toolbox from GitHub as mentioned in 'Methods'. Data will be made available on request.

Declaration of Competing Interest

No conflicts of interest.

Credit authorship contribution statement

Po-Yu Fong: Conceptualization, Methodology, Formal analysis, Investigation, Writing – original draft, Writing – review & editing, Visualization. **Danny Spampinato:** Conceptualization, Methodology, Investi-

gation, Writing – review & editing, Visualization. **Kevin Michell:** Investigation. **Marco Mancuso:** Methodology, Formal analysis. **Katlyn Brown:** Investigation, Writing – review & editing. **Jaime Ibáñez:** Investigation, Writing – review & editing. **Alessandro Di Santo:** Investigation. **Anna Latorre:** Investigation. **Kailash Bhatia:** Conceptualization, Resources, Supervision. **John C Rothwell:** Conceptualization, Methodology, Resources, Writing – review & editing, Supervision, Funding acquisition. **Lorenzo Rocchi:** Conceptualization, Methodology, Resources, Writing – review & editing, Supervision.

Data availability

Data will be made available on request.

Acknowledgment

PYF was supported by the Taiwan Government Scholarship to Study Abroad (GSSA). The work was supported by Medical Research Council, United Kingdom grant MR/P006671/1 to JCR.

Supplementary materials

Supplementary material associated with this article can be found, in the online version, at doi:10.1016/j.neuroimage.2023.120188.

References

Allen, G., McColl, R., Barnard, H., Ringe, W.K., Fleckenstein, J., Cullum, C.M., 2005. Magnetic resonance imaging of cerebellar-prefrontal and cerebellar-parietal functional connectivity. Neuroimage 28, 39–48.
Bastian, B., 2016. Violin Plots for Matlab. Github Project.
Battaglia, F., Quartarone, A., Ghilardi, M.F., Dattola, R., Bagnato, S., Rizzo, V., Morgante, L., Girlanda, P., 2006. Unilateral cerebellar stroke disrupts movement preparation and motor imagery. Clin. Neurophysiol. 117, 1009–1016.
Bedard, P., Sanes, J.N., 2011. Basal ganglia-dependent processes in recalling learned visual-motor adaptations. Exp. Brain Res. 209, 385–393.
Benagiano, V., Rizzi, A., Lorusso, L., Flace, P., Saccia, M., Cagiano, R., Ribatti, D., Roncali, L., Ambrosi, G., 2018. The functional anatomy of the cerebrocerebellar circuit: a review and new concepts. J. Comput. Neurol. 526, 769–789.
Benjamini, Y., Hochberg, Y., 1995. Controlling the false discovery rate: a practical and powerful approach to multiple testing. J. R. Stat. Soc. Ser. B (Methodol.) 57, 289–300.
Bernard, J.A., Seidler, R.D., 2013. Cerebellar contributions to visuomotor adaptation and motor sequence learning: an ALE meta-analysis. Front. Hum. Neurosci. 7, 27.
Biabani, M., Fornito, A., Mutanen, T.P., Morrow, J., Rogasch, N.C., 2019. Characterizing and minimizing the contribution of sensory inputs to TMS-evoked potentials. Brain Stimul. 12, 1537–1552.
Boukrina, O., Chen, P., 2021. Neural mechanisms of prism adaptation in healthy adults and individuals with spatial neglect after unilateral stroke: a review of fMRI studies. Brain Sci 11, 1468.
Caligiore, D., Arbib, M.A., Miall, R.C., Baldassarre, G., 2019. The super-learning hypothesis: integrating learning processes across cortex, cerebellum and basal ganglia. Neurosci. Biobehav. Rev. 100, 19–34.
Çan, M.K., Laakso, I., Nieminen, J.O., Murakami, T., Ugawa, Y., 2018. Coil model comparison for cerebellar transcranial magnetic stimulation. Biomed. Phys. Eng. Express 5, 015020.
Casula, E.P., Rocchi, L., Hannah, R., Rothwell, J.C., 2018. Effects of pulse width, waveform and current direction in the cortex: a combined cTMS-EEG study. Brain Stimul. 11, 1063–1070.
Conde, V., Tomasevic, L., Akopian, I., Stanek, K., Saturnino, G.B., Thielscher, A., Bergmann, T.O., Siebner, H.R., 2019. The non-transcranial TMS-evoked potential is an inherent source of ambiguity in TMS-EEG studies. Neuroimage 185, 300–312.
Daskalakis, Z.J., Paradiso, G.O., Christensen, B.K., Fitzgerald, P.B., Gunraj, C., Chen, R., 2004. Exploring the connectivity between the cerebellum and motor cortex in humans. J. Physiol. 557, 689–700.
de Winter, J.C., Gosling, S.D., Potter, J., 2016. Comparing the Pearson and Spearman correlation coefficients across distributions and sample sizes: a tutorial using simulations and empirical data. Psychol. Methods 21, 273–290.
Delorme, A., Makeig, S., 2004. EEGLAB: an open source toolbox for analysis of single-trial EEG dynamics including independent component analysis. J. Neurosci. Methods 134, 9–21.
Delorme, A., Mullen, T., Kothe, C., Akalin Acar, Z., Bigdely-Shamlo, N., Vankov, A., Makeig, S., 2011. EEGLAB, SIFT, NFT, BCILAB, and ERICA: new tools for advanced EEG processing. Comput. Intell. Neurosci. 2011, 130714.
Di Biasio, F., Conte, A., Bologna, M., Iezzi, E., Rocchi, L., Modugno, N., Berardelli, A., 2015. Does the cerebellum intervene in the abnormal somatosensory temporal discrimination in Parkinson's disease? Parkinsonism Relat. Disord. 21, 789–792.
Doyon, J., Bellec, P., Amsel, R., Penhune, V., Monchi, O., Carrier, J., Lehericy, S., Benali, H., 2009. Contributions of the basal ganglia and functionally related brain structures to motor learning. Behav. Brain Res. 199, 61–75.
Du, X., Rowland, L.M., Summerfelt, A., Choa, F.S., Wittenberg, G.F., Wisner, K., Wijtenburg, A., Chiappelli, J., Kochunov, P., Hong, L.E., 2018. Cerebellar-stimulation evoked prefrontal electrical synchrony is modulated by GABA. Cerebellum 17, 550–563.
Fernandez, L., Biabani, M., Do, M., Opie, G.M., Hill, A.T., Barham, M.P., Teo, W.P., Byrne, L.K., Rogasch, N.C., Enticott, P.G., 2021. Assessing cerebellar-cortical connectivity using concurrent TMS-EEG: a feasibility study. J. Neurophysiol. 125, 1768–1787.
Fernandez, L., Major, B.P., Teo, W.P., Byrne, L.K., Enticott, P.G., 2018. The impact of stimulation intensity and coil type on reliability and tolerability of cerebellar brain inhibition (CBI) *via* dual-coil TMS. Cerebellum 17, 540–549.
Fong, P.Y., Spampinato, D., Rocchi, L., Hannah, R., Teng, Y., Di Santo, A., Shoura, M., Bhatia, K., Rothwell, J.C., 2021. Two forms of short-interval intracortical inhibition in human motor cortex. Brain Stimul. 14, 1340–1352.
Galea, J.M., Jayaram, G., Ajagbe, L., Celnik, P., 2009. Modulation of cerebellar excitability by polarity-specific noninvasive direct current stimulation. J. Neurosci. 29, 9115–9122.
Galea, J.M., Mallia, E., Rothwell, J., Diedrichsen, J., 2015. The dissociable effects of punishment and reward on motor learning. Nat. Neurosci. 18, 597–602.
Galea, J.M., Vazquez, A., Pasricha, N., de Xivry, J.J., Celnik, P., 2011. Dissociating the roles of the cerebellum and motor cortex during adaptive learning: the motor cortex retains what the cerebellum learns. Cereb. Cortex 21, 1761–1770.
Gassmann, L., Gordon, P.C., Ziemann, U., 2022. Assessing effective connectivity of the cerebellum with cerebral cortex using TMS-EEG. Brain Stimul 15, 1354–1369.
Gordon, P.C., Jovellar, D.B., Song, Y., Zrenner, C., Belardinelli, P., Siebner, H.R., Ziemann, U., 2021. Recording brain responses to TMS of primary motor cortex by EEG - utility of an optimized sham procedure. Neuroimage 245, 118708.
Haar, S., Donchin, O., Dinstein, I., 2015. Dissociating visual and motor directional selectivity using visuomotor adaptation. J. Neurosci. 35, 6813–6821.
Hallett, M., Di Iorio, R., Rossini, P.M., Park, J.E., Chen, R., Celnik, P., Strafella, A.P., Matsumoto, H., Ugawa, Y., 2017. Contribution of transcranial magnetic stimulation to assessment of brain connectivity and networks. Clin. Neurophysiol. 128, 2125–2139.
Halsband, U., Lange, R.K., 2006. Motor learning in man: a review of functional and clinical studies. J. Physiol. Paris 99, 414–424.
Hardwick, R.M., Lesage, E., Miall, R.C., 2014. Cerebellar transcranial magnetic stimulation: the role of coil geometry and tissue depth. Brain Stimul. 7, 643–649.
Hernandez-Pavon, J.C., Veniero, D., Bergmann, T.O., Belardinelli, P., Bortoletto, M., Casarotto, S., Casula, E.P., Farzan, F., Fecchio, M., Julkunen, P., Kallioniemi, E., Lioumis, P., Metsomaa, J., Miniussi, C., Mutanen, T.P., Rocchi, L., Rogasch, N.C., Shafi, M.M., Siebner, H.R., Thut, G., Zrenner, C., Ziemann, U., Ilmoniemi, R.J., 2023. TMS combined with EEG: recommendations and open issues for data collection and analysis. Brain Stimul. 16, 567–593.
Kerwin, L.J., Keller, C.J., Wu, W., Narayan, M., Etkin, A., 2018. Test-retest reliability of transcranial magnetic stimulation EEG evoked potentials. Brain Stimul. 11, 536–544.
King, T.S., Chinchilli, V.M., Carrasco, J.L., 2007. A repeated measures concordance correlation coefficient. Stat. Med. 26, 3095–3113.
Klein, J., Roach, N., Burdet, E., 2014. 3DOM: a 3 degree of freedom manipulandum to investigate redundant motor control. IEEE Trans. Haptics. 7, 229–239.
Koch, G., Esposito, R., Motta, C., Casula, E.P., Di Lorenzo, F., Bonni, S., Cinnera, A.M., Ponzo, V., Maiella, M., Picazio, S., Assogna, M., Sallustio, F., Caltagirone, C., Pellicciari, M.C., 2020. Improving visuo-motor learning with cerebellar theta burst stimulation: behavioral and neurophysiological evidence. Neuroimage 208, 116424.
Krakauer, J.W., Ghez, C., Ghilardi, M.F., 2005. Adaptation to visuomotor transformations: consolidation, interference, and forgetting. J. Neurosci. 25, 473–478.
Krienen, F.M., Buckner, R.L., 2009. Segregated fronto-cerebellar circuits revealed by intrinsic functional connectivity. Cereb. Cortex 19, 2485–2497.
Lehmann, D., Skrandies, W., 1980. Reference-free identification of components of checkerboard-evoked multichannel potential fields. Electroencephalogr. Clin. Neurophysiol. 48, 609–621.
Lin, L.I., 1989. A concordance correlation coefficient to evaluate reproducibility. Biometrics 45, 255–268.
Mancuso, M., Sveva, V., Cruciani, A., Brown, K., Ibanez, J., Rawji, V., Casula, E., Premoli, I., D'Ambrosio, S., Rothwell, J., Rocchi, L., 2021. Transcranial evoked potentials can be reliably recorded with active electrodes. Brain Sci. 11, 145.
Maris, E., Oostenveld, R., 2007. Nonparametric statistical testing of EEG- and MEG-data. J. Neurosci. Methods 164, 177–190.
Massimini, M., Ferrarelli, F., Huber, R., Esser, S.K., Singh, H., Tononi, G., 2005. Breakdown of cortical effective connectivity during sleep. Science 309, 2228–2232.
Matsumoto, H., Hanajima, R., Hamada, M., Terao, Y., Yugeta, A., Inomata-Terada, S., Nakatani-Enomoto, S., Tsuji, S., Ugawa, Y., 2008. Double-pulse magnetic brain stem stimulation: mimicking successive descending volleys. J. Neurophysiol. 100, 3437–3444.
Middleton, F.A., Strick, P.L., 2001. Cerebellar projections to the prefrontal cortex of the primate. J. Neurosci. 21, 700–712.
Monaco, J., Rocchi, L., Ginatempo, F., D'Angelo, E., Rothwell, J.C., 2018. Cerebellar theta-burst stimulation impairs memory consolidation in eyeblink classical conditioning. Neural Plast. 2018, 6856475.
Mouraux, A., Iannetti, G.D., 2009. Nociceptive laser-evoked brain potentials do not reflect nociceptive-specific neural activity. J. Neurophysiol. 101, 3258–3269.
Nezafat, R., Shadmehr, R., Holcomb, H.H., 2001. Long-term adaptation to dynamics of reaching movements: a PET study. Exp. Brain Res. 140, 66–76.
Oldfield, R.C., 1971. The assessment and analysis of handedness: the Edinburgh inventory. Neuropsychologia 9, 97–113.
Oostenveld, R., Fries, P., Maris, E., Schoffelen, J.M., 2011. FieldTrip: open source software for advanced analysis of MEG, EEG, and invasive electrophysiological data. Comput. Intell. Neurosci. 2011, 156869.

Opie, G.M., Rogasch, N.C., Goldsworthy, M.R., Ridding, M.C., Semmler, J.G., 2017. Investigating TMS-EEG indices of long-interval intracortical inhibition at different interstimulus intervals. Brain Stimul. 10, 65–74.
Palesi, F., De Rinaldis, A., Castellazzi, G., Calamante, F., Muhlert, N., Chard, D., Tournier, J.D., Magenes, G., D'Angelo, E., Gandini Wheeler-Kingshott, C.A.M., 2017. Contralateral cortico-ponto-cerebellar pathways reconstruction in humans *in vivo*: implications for reciprocal cerebro-cerebellar structural connectivity in motor and non–motor areas. Sci. Rep. 7, 12841.
Palesi, F., Tournier, J.D., Calamante, F., Muhlert, N., Castellazzi, G., Chard, D., D'Angelo, E., Wheeler-Kingshott, C.A., 2015. Contralateral cerebello-thalamo-cortical pathways with prominent involvement of associative areas in humans *in vivo*. Brain Struct. Funct. 220, 3369–3384.
Pernet, C.R., Latinus, M., Nichols, T.E., Rousselet, G.A., 2015. Cluster-based computational methods for mass univariate analyses of event-related brain potentials/fields: a simulation study. J. Neurosci. Methods 250, 85–93.
Pinto, A.D., Chen, R., 2001. Suppression of the motor cortex by magnetic stimulation of the cerebellum. Exp. Brain Res. 140, 505–510.
Rawji, V., Kaczmarczyk, I., Rocchi, L., Fong, P.Y., Rothwell, J.C., Sharma, N., 2021. Preconditioning stimulus intensity alters paired-pulse TMS evoked potentials. Brain Sci. 11, 326.
Reis, J., Swayne, O.B., Vandermeeren, Y., Camus, M., Dimyan, M.A., Harris-Love, M., Perez, M.A., Ragert, P., Rothwell, J.C., Cohen, L.G., 2008. Contribution of transcranial magnetic stimulation to the understanding of cortical mechanisms involved in motor control. J. Physiol. 586, 325–351.
Rocchi, L., Di Santo, A., Brown, K., Ibanez, J., Casula, E., Rawji, V., Di Lazzaro, V., Koch, G., Rothwell, J., 2021. Disentangling EEG responses to TMS due to cortical and peripheral activations. Brain Stimul. 14, 4–18.
Rocchi, L., Ibanez, J., Benussi, A., Hannah, R., Rawji, V., Casula, E., Rothwell, J., 2018. Variability and predictors of response to continuous theta burst stimulation: a TMS-EEG study. Front. Neurosci. 12, 400.
Rocchi, L., Latorre, A., Ibanez Pereda, J., Spampinato, D., Brown, K.E., Rothwell, J., Bhatia, K., 2019. A case of congenital hypoplasia of the left cerebellar hemisphere and ipsilateral cortical myoclonus. Mov. Disord. 34, 1745–1747.
Rogasch, N.C., Sullivan, C., Thomson, R.H., Rose, N.S., Bailey, N.W., Fitzgerald, P.B., Farzan, F., Hernandez-Pavon, J.C., 2017. Analysing concurrent transcranial magnetic stimulation and electroencephalographic data: a review and introduction to the open–source TESA software. Neuroimage 147, 934–951.
Rogasch, N.C., Thomson, R.H., Daskalakis, Z.J., Fitzgerald, P.B., 2013. Short-latency artifacts associated with concurrent TMS-EEG. Brain Stimul. 6, 868–876.
Rogasch, N.C., Thomson, R.H., Farzan, F., Fitzgibbon, B.M., Bailey, N.W., Hernandez–Pavon, J.C., Daskalakis, Z.J., Fitzgerald, P.B., 2014. Removing artefacts from TMS-EEG recordings using independent component analysis: importance for assessing prefrontal and motor cortex network properties. Neuroimage 101, 425–439.
Ross, J.M., Ozdemir, R.A., Lian, S.J., Fried, P.J., Schmitt, E.M., Inouye, S.K., Pascual-Leone, A., Shafi, M.M., 2022. A structured ICA-based process for removing auditory evoked potentials. Sci. Rep. 12, 1391.
Rossi, S., Hallett, M., Rossini, P.M., Pascual-Leone, A., Safety of, T.M.S.C.G., 2009. Safety, ethical considerations, and application guidelines for the use of transcranial magnetic stimulation in clinical practice and research. Clin. Neurophysiol. 120, 2008–2039.
Rossini, P.M., Burke, D., Chen, R., Cohen, L.G., Daskalakis, Z., Di Iorio, R., Di Lazzaro, V., Ferreri, F., Fitzgerald, P.B., George, M.S., Hallett, M., Lefaucheur, J.P., Langguth, B., Matsumoto, H., Miniussi, C., Nitsche, M.A., Pascual-Leone, A., Paulus, W., Rossi, S., Rothwell, J.C., Siebner, H.R., Ugawa, Y., Walsh, V., Ziemann, U., 2015. Non-invasive electrical and magnetic stimulation of the brain, spinal cord, roots and peripheral nerves: basic principles and procedures for routine clinical and research application. An updated report from an I.F.C.N. Committee. Clin. Neurophysiol. 126, 1071–1107.
Sasaki, R., Hand, B.J., Liao, W.Y., Rogasch, N.C., Fernandez, L., Semmler, J.G., Opie, G.M., 2022. Utilising TMS-EEG to assess the response to cerebellar-brain inhibition. Cerebellum.
Schlerf, J.E., Galea, J.M., Spampinato, D., Celnik, P.A., 2015. Laterality differences in cerebellar-motor cortex connectivity. Cereb. Cortex 25, 1827–1834.
Shadmehr, R., Holcomb, H.H., 1997. Neural correlates of motor memory consolidation. Science 277, 821–825.
Spampinato, D., Avci, E., Rothwell, J., Rocchi, L., 2021. Frequency-dependent modulation of cerebellar excitability during the application of non-invasive alternating current stimulation. Brain Stimul. 14, 277–283.
Spampinato, D., Celnik, P., 2021. Multiple motor learning processes in humans: defining their neurophysiological bases. Neuroscientist 27, 246–267.
Spampinato, D., Ibanez, J., Spanoudakis, M., Hammond, P., Rothwell, J.C., 2020a. Cerebellar transcranial magnetic stimulation: the role of coil type from distinct manufacturers. Brain Stimul. 13, 135–156.
Spampinato, D.A., Block, H.J., Celnik, P.A., 2017. Cerebellar-M1 connectivity changes associated with motor learning are somatotopic specific. J. Neurosci. 37, 2377–2386.
Spampinato, D.A., Celnik, P.A., Rothwell, J.C., 2020b. Cerebellar-motor cortex connectivity: one or two different networks? J. Neurosci. 40, 4230–4239.
Strata, P., 2015. The emotional cerebellum. Cerebellum 14, 570–577.
Strick, P.L., Dum, R.P., Fiez, J.A., 2009. Cerebellum and nonmotor function. Annu. Rev. Neurosci. 32, 413–434.
Striemer, C.L., Enns, J.T., Whitwell, R.L., 2019. Visuomotor adaptation in the absence of input from early visual cortex. Cortex 115, 201–215.
Taylor, J.A., Ivry, R.B., 2014. Cerebellar and prefrontal cortex contributions to adaptation, strategies, and reinforcement learning. Prog. Brain Res. 210, 217–253.
ter Braack, E.M., de Vos, C.C., van Putten, M.J., 2015. Masking the auditory evoked potential in TMS-EEG: a comparison of various methods. Brain Topogr. 28, 520–528.
Tremblay, S., Rogasch, N.C., Premoli, I., Blumberger, D.M., Casarotto, S., Chen, R., Di Lazzaro, V., Farzan, F., Ferrarelli, F., Fitzgerald, P.B., Hui, J., Ilmoniemi, R.J., Kimiskidis, V.K., Kugiumtzis, D., Lioumis, P., Pascual-Leone, A., Pellicciari, M.C., Rajji, T., Thut, G., Zomorrodi, R., Ziemann, U., Daskalakis, Z.J., 2019. Clinical utility and prospective of TMS-EEG. Clin. Neurophysiol. 130, 802–844.
Tzvi, E., Koeth, F., Karabanov, A.N., Siebner, H.R., Kramer, U.M., 2020. Cerebellar - premotor cortex interactions underlying visuomotor adaptation. Neuroimage 220, 117142.
Tzvi, E., Loens, S., Donchin, O., 2021. Mini-review: the role of the cerebellum in visuomotor adaptation. Cerebellum 21, 306–313.
Ugawa, Y., Uesaka, Y., Terao, Y., Hanajima, R., Kanazawa, I., 1995. Magnetic stimulation over the cerebellum in humans. Ann. Neurol. 37, 703–713.
van den Hurk, P., Mars, R.B., van Elswijk, G., Hegeman, J., Pasman, J.W., Bloem, B.R., Toni, I., 2007. Online maintenance of sensory and motor representations: effects on corticospinal excitability. J. Neurophysiol. 97, 1642–1648.
van Elswijk, G., Schot, W.D., Stegeman, D.F., Overeem, S., 2008. Changes in corticospinal excitability and the direction of evoked movements during motor preparation: a TMS study. BMC Neurosci. 9, 51.
Watson, T.C., Becker, N., Apps, R., Jones, M.W., 2014. Back to front: cerebellar connections and interactions with the prefrontal cortex. Front. Syst. Neurosci. 8, 4.
Werhahn, K.J., Taylor, J., Ridding, M., Meyer, B.U., Rothwell, J.C., 1996. Effect of transcranial magnetic stimulation over the cerebellum on the excitability of human motor cortex. Electroencephalogr. Clin. Neurophysiol. 101, 58–66.
Wessel, M.J., Draaisma, L.R., Morishita, T., Hummel, F.C., 2019. The effects of stimulator, waveform, and current direction on intracortical inhibition and facilitation: a TMS comparison study. Front. Neurosci. 13, 703.

Supplementary material 1 -Methodology of CBI

Cerebellar-brain inhibition protocol

In the present study, CBI was tested in experiments 1 and 4 to ensure the cerebellar intensity was enough to inhibit the contralateral motor cortex. In experiment 1, we recorded single pulse MEPs from the contralateral M1 (LM1-TS, RM1-TS) and conditioned MEP in CBI for each hemisphere (L-CBI: RCS and LM1-TS; R-CBI: LCS and RM1-TS). The conditions M1-TS and CBI on each side were implemented in each block of cerebellar TEP (i.e., block 1 consisted of LM1-TS, RCS, and L-CBI; block 2 was composed of RM1-TS, LCS, and R-CBI). The three conditions in each block were recorded in pseudorandomized order. Each condition consisted of 100 pulses, delivered at an inter-trial interval (ITI) of 5 s ± 10%, meaning 4.5-5.5 s. Participants had a 5-minute break every 100 trials to avoid coil overheating and discomfort. In experiment 4, we tested a short block of CBI before the behavioural experiment, to ensure that cerebellar intensity was sufficient to elicit a reliable CBI. Each condition included 15 trials for both LM1-TS and L-CBI conditions, and the ITI was the same as experiment 1, 5 s ± 10%.

Electromyography recording

Surface electromyography (EMG) was recorded from the first dorsal interosseous (FDI) muscle of both hands by means of adhesive electrodes (WhiteSensor 40713, AmbuR, Denmark) arranged in a belly-tendon montage. Signals were amplified (gain 1000x) and bandpass filtered (5 Hz - 3000Hz) with a Digitimer D360 amplifier (Digitimer Ltd, Welwyn Garden City, Hers, UK). They were sampled at 5000 Hz through a Power1401 data acquisition interface (Cambridge Electronic Design Ltd., Cambridge, UK) and displayed by Signal software version 7.01 (Cambridge Electronic Design Ltd., Cambridge, UK).

Transcranial magnetic stimulation

Monophasic TMS pulses were delivered via two Magstim 200^2 stimulators (Magstim, Whitland, Dyfed, UK). For stimulation of M1, we used a 70 mm figure-of-eight coil (D70α, Magstim, UK), with the handle pointing backwards 45° to the midline, inducing current in the brain in the posterior-anterior direction. TMS was delivered over the cortical hotspot, defined as the location in M1 where the largest motor evoked potential (MEP) in the contralateral FDI could be obtained. Stimulation was delivered at an intensity able to elicit a MEP of approximately 1 mV amplitude in the contralateral relaxed FDI muscle (conditions: LM1-TS,

RM1-TS, L-CBI, and R-CBI).

CBI was tested on the FDI muscle with a standard paired-pulse TMS paradigm, consisting of a test stimulus (TS) applied over M1 with a 70 mm figure-of-eight coil (D70α, Magstim, UK), at an intensity able to induce a MEP of around 1 mV amplitude, preceded by a conditioning stimulus (CS) applied with a 110 mm double cone coil (Magstim, Whitland, Dyfed, UK) over the contralateral cerebellar hemisphere 5 ms before the TS (Rocchi et al., 2019; Spampinato et al., 2021; Spampinato et al., 2020). The location of the double cone coil for cerebellar conditioning was the same as the single pulse cerebellar TMS in experiment 1 and 4. The intensity of the CS was set at AMT_{BA}-5% MSO, which is the same as the intensity for RCS and LCS.

Data processing and statistics

Peak-to-peak MEP amplitudes were measured offline. Similar to previous studies (Fong et al., 2021; Spampinato et al., 2021; van den Hurk et al., 2007; van Elswijk et al., 2008; Wessel et al., 2019), trials containing background EMG activity > 50 μV in the 100 ms preceding the TMS pulse were excluded. CBI was calculated as the ratio of conditioned to test MEP amplitudes, with values

greater than 1 indicating no inhibition and those close to 0 representing strong inhibition.

Normality of distribution was examined by the Kolmogorov-Smirnov test. To assess CBI, two Wilcoxon signed rank tests were applied in experiment 1 (LM1-TS vs L-CBI; RM1-TS vs R-CBI) because of non-normal distribution (LM1-TS in experiment 1: $p = 0.024$; L-CBI in experiment 1: $p = 0.006$; RM1-TS in experiment 1: $p = 0.04$; R-CBI in experiment 1: $p = 0.003$). One paired t-test was performed in experiment 4 (LM1-TS vs L-CBI). P values < 0.05 were considered significant. Statistical analyses for MEP data were performed with SPSS version 22 (IBM, USA).

Reference

Fong, P.Y., Spampinato, D., Rocchi, L., Hannah, R., Teng, Y., Di Santo, A., Shoura, M., Bhatia, K., Rothwell, J.C., 2021. Two forms of short-interval intracortical inhibition in human motor cortex. Brain Stimul 14, 1340-1352.

Rocchi, L., Latorre, A., Ibanez Pereda, J., Spampinato, D., Brown, K.E., Rothwell, J., Bhatia, K., 2019. A case of congenital hypoplasia of the left cerebellar hemisphere and ipsilateral cortical myoclonus. Mov Disord 34, 1745-1747.

Spampinato, D., Avci, E., Rothwell, J., Rocchi, L., 2021. Frequency-dependent modulation of cerebellar excitability during the application of non-invasive alternating current stimulation. Brain Stimul 14, 277-283.

Spampinato, D., Ibanez, J., Spanoudakis, M., Hammond, P., Rothwell, J.C., 2020. Cerebellar transcranial magnetic stimulation: The role of coil type from distinct manufacturers. Brain Stimul.

van den Hurk, P., Mars, R.B., van Elswijk, G., Hegeman, J., Pasman, J.W., Bloem, B.R., Toni, I., 2007. Online maintenance of sensory and motor representations: effects on corticospinal excitability. J Neurophysiol 97, 1642-1648.
van Elswijk, G., Schot, W.D., Stegeman, D.F., Overeem, S., 2008. Changes in corticospinal excitability and the direction of evoked movements during motor preparation: a TMS study. BMC Neurosci 9, 51.
Wessel, M.J., Draaisma, L.R., Morishita, T., Hummel, F.C., 2019. The Effects of Stimulator, Waveform, and Current Direction on Intracortical Inhibition and Facilitation: A TMS Comparison Study. Front Neurosci 13, 703.

Supplementary material 2 – intensities of cerebellar TMS

Subject	Brainstem AMT (AMT_{BS}) (%MSO)	Stimulation intensity (%MSO)
1		75%
2		70%
3		75%
4		80%
5		70%
6	65%	60%
7		60%
8		70%
9	70%	65%
10		70%
11	60%	55%
12		65%
13	70%	65%
14		65%
15		75%
16		70%
17		75%
18	65%	60%
19	70%	65%
20		70%
21	70%	65%
22	65%	60%
23	50%	45%
24		55%
25		65%
26	70%	65%
27		75%
28	75%	70%
29		55%
30	70%	65%
31		50%
32		60%
Mean	66.7%	66.0%
SD	6.5%	7.8%

Table S1. Only twelve participants had measurable brainstem AMT (AMT_{BS}) in the present study. All participants` intensities for cerebellar TMS are also shown in the table.

Supplementary Material 3 - Measurement of the induced voltage from different coils

To check that e-field in deep cerebellar structure by the coils (i.e., 110mm DC uncoated coil, D70 alpha F8 coil, D50 alpha uncoated F8 coil), we used a pickup coil (Search Coil, radius 6.18mm, Magstim, UK) to record outputs from each stimulating coil. According to a study including magnetic resonance imaging scans from 100 subjects, the cerebellar motor area is located in lobules V and VIII, about 3-3.5 cm from the scalp (Hardwick et al., 2014). Therefore, the induced voltage measurement for the F8 coil was performed by placing the centre of the search coil at 3.5 cm from the centre of the stimulating coil. For the DC coil, the centre of the coil usually cannot contact the scalp, meaning that an air gap between the centre of DC coil and the scalp is present. To measure the distance of the gap, we inserted a blu tack into the air gap between the centre of the DC coil and the EEG cap. The distance was about 16 mm (Fig.S2A). Therefore, the induced voltage measurement for DC coil was set by placing the centre of the search coil at 5.1 cm (i.e. 3.5 + 1.6 cm)from the centre of the DC coil. The intensities ranged from 45% MSO to 80% MSO, in steps of 5% MSO.

The induced voltage was recorded with a digital oscilloscope (Owon, 100MHz, Fujian Lilliput Optoelectronics Technology Co., Ltd., China). We could then plot the results from each coil (Fig.S2B) and their individual waveforms (Fig. S2C). The details of the recording data are listed below:

DC coil			
Intensity (%MSO)	Difference (V)	Peak (V)	Trough (V)
45	5.7	4.1	-1.6
50	6.4	4.6	-1.8
55	7.0	5.0	-2.0
60	7.5	5.4	-2.1
65	8.1	5.9	-2.2
70	8.7	6.3	-2.4
75	9.4	6.9	-2.6
80	10.0	7.3	-2.7
D50 alpha F8 coil			
Intensity (%MSO)	Difference (V)	Peak (V)	Trough (V)
45	3.8	2.6	-1.2
50	4.2	3.0	-1.2
55	4.6	3.2	-1.4

60	5.0	3.6	-1.4
65	5.2	3.8	-1.4
70	5.8	4.2	-1.6
75	6.0	4.4	-1.6
80	6.6	4.8	-1.8
D70 alpha F8 coil			
Intensity (%MSO)	Difference (V)	Peak (V)	Trough (V)
45	4.0	2.9	-1.1
50	4.3	3.1	-1.2
55	4.8	3.4	-1.4
60	5.2	3.8	-1.4
65	5.7	4.1	-1.6
70	6.2	4.5	-1.7
75	6.6	4.8	-1.8
80	7.0	5.1	-1.9

Reference

Hardwick, R.M., Lesage, E., Miall, R.C., 2014. Cerebellar transcranial magnetic stimulation: the role of coil geometry and tissue depth. Brain Stimul 7, 643-649.

(A)LcbTEP_AEP

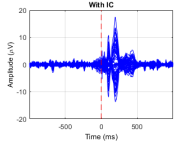

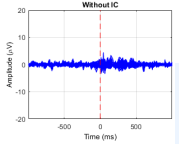

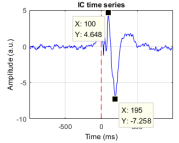

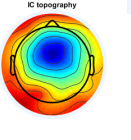

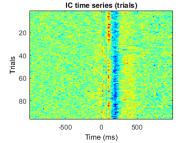

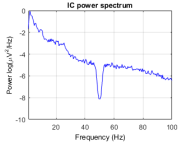

IC 1 of 19

Var. accounted for: 87.9 %

Figure options

Time (ms)	-999 999
Freq. (Hz)	1 100
Amp. (uV)	-20 20
Amp. (a.u.)	-10 5

Update figures

Scroll ICs by trial

Scroll ICs

IC classification

Keep

Next IC: 2

Back Next

(B)RcbTEP_AEP

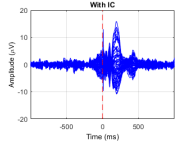

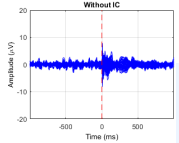

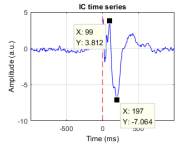

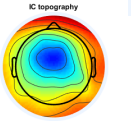

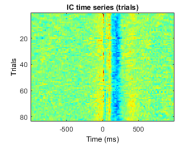

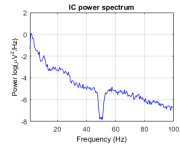

IC 1 of 20

Var. accounted for: 81.5 %

Figure options

Time (ms)	-999 999
Freq. (Hz)	1 100
Amp. (uV)	-20 20
Amp. (a.u.)	-10 5

Update figures

Scroll ICs by trial

Scroll ICs

IC classification

Keep

Next IC: 2

Back Next

(A)

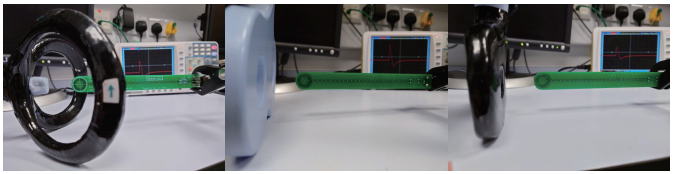
DC coil
D70 alpha coil
D50 alpha coil

(B)

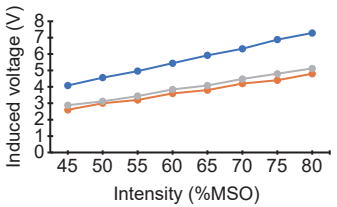
Induced voltage (V)
0
1
2
3
4
5
6
7
8
45
50
55
60
65
70
75
80
Intensity (%MSO)

(C)

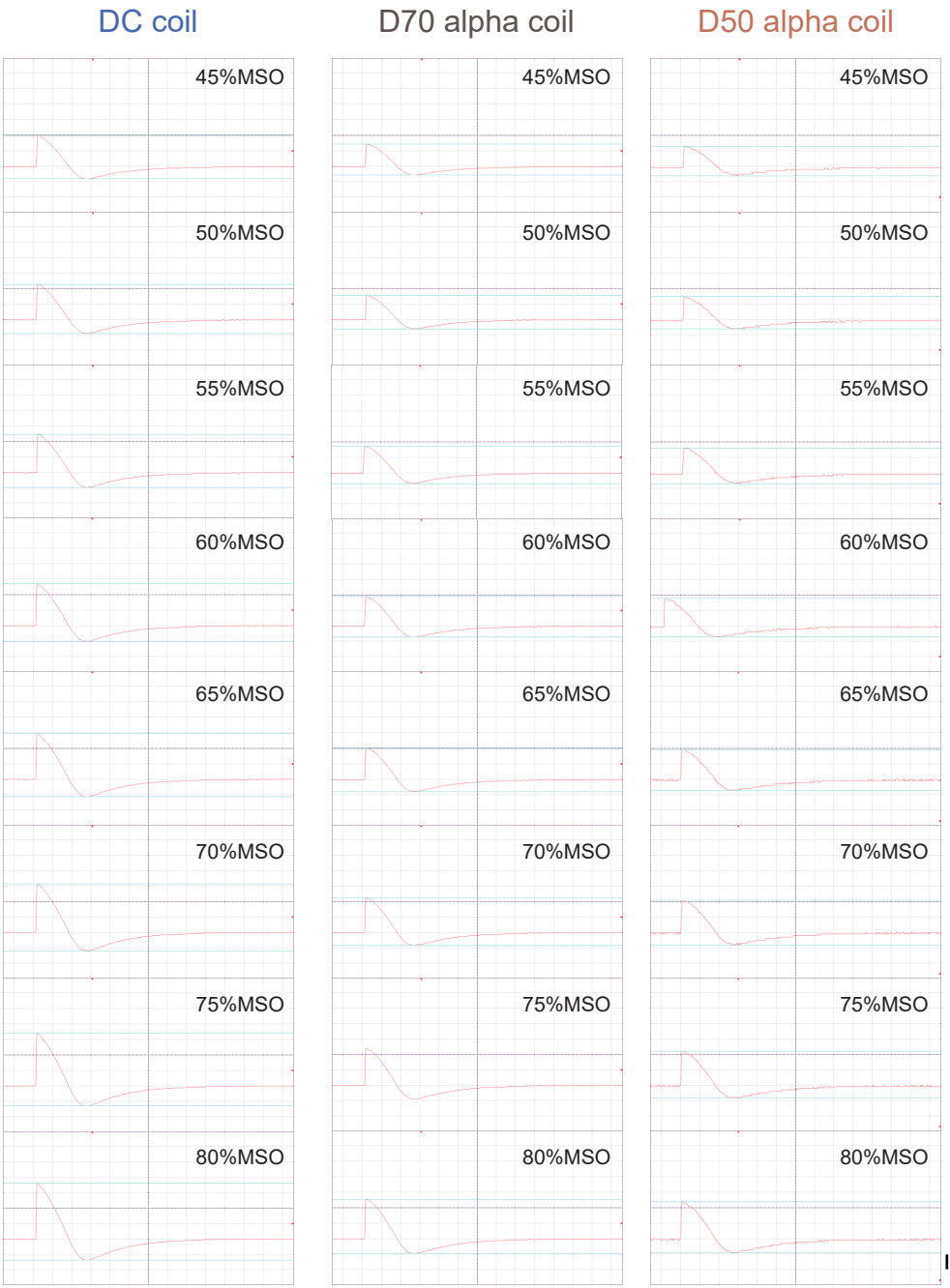
DC coil
D70 alpha coil
D50 alpha coil
45%MSO
50%MSO
55%MSO
60%MSO
65%MSO
70%MSO
75%MSO
80%MSO
2V
50us

Supplementary figure captions

Fig.S1. Demonstration of AEP component in ICA

The upper panel represents an AEP component after the second round of ICA of LcbTEP_AEP from one representative participant (A). The bottom panel indicates an AEP component after the second ICA of RcbTEP_AEP from the same participant (B).

Fig.S2. Measurement of induced voltage by three different coils.

The upper left panel shows the setup of the induced voltage measurement 3.5 cm away from the coil focus (110mm DC coil, D70 alpha figure-of-eight coil, and D50 alpha figure-of-eight coil). Note that a blu tack on the central region of the DC coil was used to measure the gap between the central point of the DC coil to the scalp of a researcher`s head (1.6 cm, see details in supplementary material 4). Therefore, the DC coil was measured at 5.1cm (1.6 cm +3.5 cm) (A). The upper right panel illustrates the recordings of induced voltage from 45% MSO to 80% MSO of each coil. The blue line is the DC coil. The grey line is the D70 alpha figure-of-eight coil. The orange line is the D50 alpha figure-of-eight coil (B). The bottom panel presents the waveforms of each coil at each intensity (C).